Neural populations in the language network differ in the size of their temporal receptive windows

Tamar I. Regev[1,2*], Colton Casto[1,2,3,4*], Eghbal A. Hosseini[1,2], Markus Adamek[5,6], Anthony L. Ritaccio[7], Jon T. Willie[5,6], Peter Brunner[5,6,8] and Evelina Fedorenko[1,2,3]

[1] Brain and Cognitive Sciences Department, Massachusetts Institute of Technology, Cambridge MA
[2] McGovern Institute for Brain Research, Massachusetts Institute of Technology, Cambridge MA
[3] Program in Speech and Hearing Bioscience and Technology (SHBT), Harvard University, Boston MA
[4] Kempner Institute for the Study of Natural and Artificial Intelligence, Harvard University, Allston MA
[5] National Center for Adaptive Neurotechnologies, Albany NY
[6] Department of Neurosurgery, Washington University School of Medicine, St. Louis MO
[7] Department of Neurology, Mayo Clinic, Jacksonville FL
[8] Department of Neurology, Albany Medical College, Albany NY

* Equal contribution

Correspondence should be sent to: tamarr@mit.edu; ccasto@mit.edu; evelina9@mit.edu

Abstract

Language comprehension is fast and seemingly effortless. However, in spite of long knowing what brain regions enable this feat, our knowledge of the precise neural computations that these frontal and temporal regions implement remains limited. One highly controversial question is whether functional differences exist among the neural populations that comprise the language network. Leveraging the high spatiotemporal resolution of intracranial recordings, we clustered the timecourses of responses to sentences and linguistically degraded conditions and discovered three response profiles that robustly differ in their temporal dynamics. These profiles appear to reflect different temporal receptive windows (TRWs), with average TRWs of about 1, 4, and 6 words, as estimated with a simple one-parameter model. Neural populations exhibiting these profiles are interleaved across the language network, which suggests that all language regions have direct access to distinct, multi-scale representations of linguistic input—a property that may be critical for the efficiency and robustness of language processing.

Introduction

Language processing engages a network of brain regions that reside in the temporal and frontal lobes and are typically left-lateralized (e.g., Fedorenko et al., 2010; Pallier et al., 2011). These brain regions respond robustly to linguistic stimuli across presentation modalities (Fedorenko et al., 2010; Vagharchakian et al., 2012; Regev et al., 2013; Scott et al., 2017), tasks (Fedorenko et al., 2010; Cheung et al., 2020; Diachek, Blank, Siegelman et al., 2020), and languages (Malik-Moraleda, Ayyash et al. 2022). This language-responsive network is highly selective for language, showing little or no response to diverse non-linguistic inputs and tasks (e.g., Fedorenko et al., 2011; Monti et al., 2012; Deen et al., 2015; Ivanova et al., 2020, 2021; Liu et al., 2020; Chen et al., 2023; Shain, Paunov, Chen et al., 2023). However, the precise computations and neuronal dynamics that underlie language comprehension remain debated.

Based on neuroimaging and aphasia evidence, some have argued for dissociations among different aspects of language, including phonological/word-form processing (e.g., Okada and Hickok, 2006; Graves et al., 2008; DeWitt and Rauschecker, 2012), the processing of word meanings (e.g., Price et al., 1997; Rodd et al., 2005; Mesulam et al., 2013), and syntactic/combinatorial processing (e.g., Friederici, 2002, 2011; Hagoort, 2005; Grodzinsky and Santi, 2008; Matchin and Hickok, 2020). However, other studies have reported distributed sensitivity to these aspects of language across the language network (Fedorenko et al., 2010, 2020; Bautista and Wilson, 2016; Blank et al., 2016; Anderson et al., 2021; Caucheteux et al., 2021; Reddy & Wehbe, 2021; Shain, Blank et al., 2020; Regev et al., 2021). Some of the challenges in discovering robust functional differences within the language network may have to do with the limitations of fMRI—the dominant methodology available for studying language processing. Each fMRI voxel contains a million or more individual neurons, which may differ functionally. If different linguistic computations are implemented in distinct neural populations that are distributed and interleaved across the language cortex, such dissociations may be difficult to detect with fMRI. Further, the relatively slow temporal resolution of fMRI (typically, ~2 seconds) may obscure linguistic computations that happen on a faster timescale.

In recent years, invasive recordings of human neural activity (e.g., Mukamel and Fried, 2011), including electrocorticography (ECoG) and stereo electroencephalography (sEEG), have become increasingly available to language neuroscience researchers, as patients undergoing presurgical evaluation (usually for intractable epilepsy) agree to perform linguistic tasks while implanted with intracranial electrodes. These data have high spatial and temporal resolution, allowing the tracking of neural dynamics across both space and time.

Several previous studies have probed intracranial neural responses during language comprehension (e.g., Fedorenko et al., 2016; Nelson et al., 2017; Woolnough et al., 2023; Desbordes et al., 2023; Goldstein et al., 2022; 2023). For example, Fedorenko et al. (2016) reported sensitivity in language-responsive electrodes to both word meanings and combinatorial processing, in line with fMRI findings (e.g., Fedorenko et al., 2010; Bedny et al., 2011). They also reported a temporal profile where neural activity gradually increases (builds up) across the sentence (replicated by Nelson et al., 2017; Desbordes et al., 2023; Woolnough et al., 2023),

which they interpreted as reflecting the construction of a sentence meaning. However, considerable disagreement exists in the field regarding the number of distinct profiles that characterize cortical language responses, how they functionally differ, and what computations they collectively support in the service of language comprehension and production.

Here, we report a detailed investigation of neural responses during language processing. To isolate the language network from nearby lower-level perceptual areas and domain-general cognitive areas, we focus on electrodes that show a characteristic functional signature of the language areas: a stronger response to sentences than to sequences of nonwords (as in Fedorenko et al., 2016). To foreshadow our findings, we report three response profiles that differ in their temporal dynamics and overall magnitude of response to linguistically degraded conditions. Using a toy model with a single parameter—the timescale of information integration—we argue that these profiles reflect distinct temporal receptive window sizes in the language system (e.g., Lerner et al., 2011; Blank and Fedorenko, 2020; Jain et al., 2020).

Results

We used intracranial recordings from patients with intractable epilepsy to investigate neural responses during language comprehension. Participants in Dataset 1 were presented with four types of linguistic stimuli that have been traditionally used to tease apart neural responses to word meanings and syntactic structure (Fedorenko et al., 2010, 2012, 2016; Pallier et al., 2011; Shain, Kean et al., 2023; Desbordes et al., 2023; for earlier uses of this paradigm, see Mazoyer et al., 1993; Friederici et al., 2000; Humphries et al., 2001; Vandenberghe et al., 2002): sentences (S), lists of unconnected words (W), Jabberwocky sentences (J), and lists of unconnected nonwords (N) (**Figure 1A,B,** Methods*,* all stimuli are available at osf.io/xfbr8/). In each trial, 8 words or nonwords were presented on a screen serially and participants were asked to silently read them. To maintain alertness, after each trial, participants judged whether a probe word/nonword had appeared in that trial. See Methods for further details of stimulus presentation and behavioral response data. In Dataset 2, just two of these conditions were used: sentences and lists of nonwords.

We asked three research questions: 1) Does the language network contain reliably distinct response profiles? If so - 2) What do these profiles reflect? And finally - 3) Do electrodes exhibiting different response profiles tend to be located in particular regions of the language network? We used Dataset 1 for initial evaluation of these questions because this dataset contained a richer set of experimental conditions. We then used Dataset 2 as an attempt to replicate the findings despite the more compact experimental paradigm.

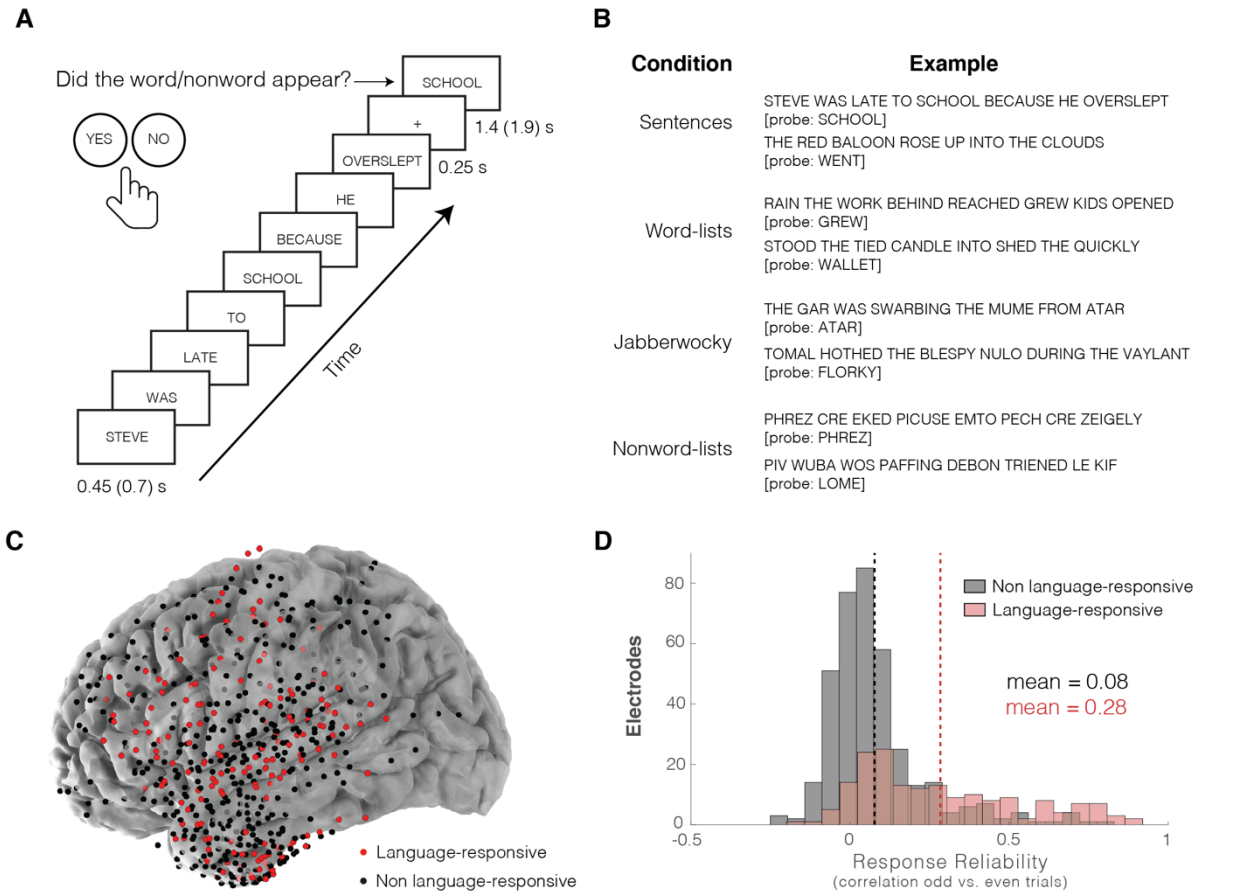

Figure 1 – Experimental procedure and the distribution of the implanted electrodes for Dataset 1. A) A sample trial from the Sentence condition. **B)** For each of the four experimental conditions, items are either presented with probes that appeared in the trial or not. Adapted from Fedorenko et al. (2016). **C)** The locations of language-responsive (n=177, red; Methods) and non-language-responsive (n=373, black) electrodes across the six participants in Dataset 1. Electrodes were implanted almost exclusively in the left hemisphere for Dataset 1 and concentrated in the temporal and frontal lobes. **D)** Response reliability across odd and even trials (based on a correlation of mean condition-level responses) for language-responsive and non-language-responsive electrodes. Language-responsive electrodes exhibit more reliable responses to linguistic stimuli than non-language-responsive electrodes.

1. Language-responsive electrodes exhibit reliably distinct response profiles.

We clustered the high gamma neural response patterns of language-responsive electrodes from Dataset 1 (6 participants, same as those used in Fedorenko et al., 2016, 177 language-responsive electrodes; **Figure 1C**, Methods, **Table 1**) to sentences (S), word-lists (W), Jabberwocky sentences (J) and nonword-lists (N) (**Figure 1A, B**). We focused on differences across experimental conditions and therefore clustering was performed on the average condition timecourses, which were concatenated across the four conditions to create a single timecourse per electrode (**Figure 2B**, Methods). The k-medoids clustering algorithm, combined with the "elbow" method (Methods), suggested that three clusters (k=3) optimally explain the data (**Figure 2A;** similar

results emerge with a k-means clustering algorithm, osf.io/xfbr8/). Although we combined the electrodes from all 6 participants for clustering, electrodes that belong to each of the three clusters are evident in every participant individually (**Figure 2B**, **S1**).

When we repeat the clustering analysis while omitting electrodes below a parametrically varying reliability threshold, the elbow at k=3 becomes more pronounced (**Figure 2A inset**). Furthermore, when clustering is performed using a larger value of k (e.g., k=10), the profiles of many of the additional clusters resemble the profiles that we discover when clustering using k=3 (**Figure S2**). And finally, responses within a given cluster—especially the more reliable ones—appear visually similar to the prototypical cluster response profiles, with only a couple highly reliable responses exhibiting a distinct profile (**Figure S3**). Taken together, these findings suggest that although the three response types we uncovered may not be the only responses that exist in the language network, they do capture a substantial amount of the functional heterogeneity.

Inspection of the average timecourse by cluster (**Figure 2E**) revealed three distinct response profiles (see **Figure 2D** for best representative electrodes from each cluster —'medoids'— chosen by the k-medoids algorithm). Cluster 1 (n=92 electrodes; range across participants: 5-34, **Figure S1**) is characterized by a relatively slow increase (build-up) of neural activity across the 8 words in the S condition (a pattern similar to the one reported by Fedorenko et al., 2016; Nelson et al., 2017; Desbordes et al., 2023; Woolnough et al., 2023; but see Discussion), and much lower activity for the W, J, and N conditions, with no difference between the J and N conditions (**Figure 2F**). Cluster 2 (n=67 electrodes; range across participants: 1-21, **Figure S1**) displays a quicker build-up of neural activity in the S condition that plateaus approximately 3 words into the sentence, a quick build-up of activity in the W condition that begins to decay after the third word, and a similar response to the J and N conditions as to the W condition with an overall lower magnitude. Cluster 2 also exhibits 'locking' of the neural activity to the onsets of individual words in the S condition. Finally, Cluster 3 (n=18 electrodes; range across participants: 1-7, **Figure S1**) shows no build-up of activity, and is instead characterized by a high degree of locking to the onset of each word or nonword in all conditions. Additionally, the response magnitudes of Cluster 3 are more similar across conditions compared to the other two clusters, although the S>W>J>N pattern is still present (**Figure 2F**).

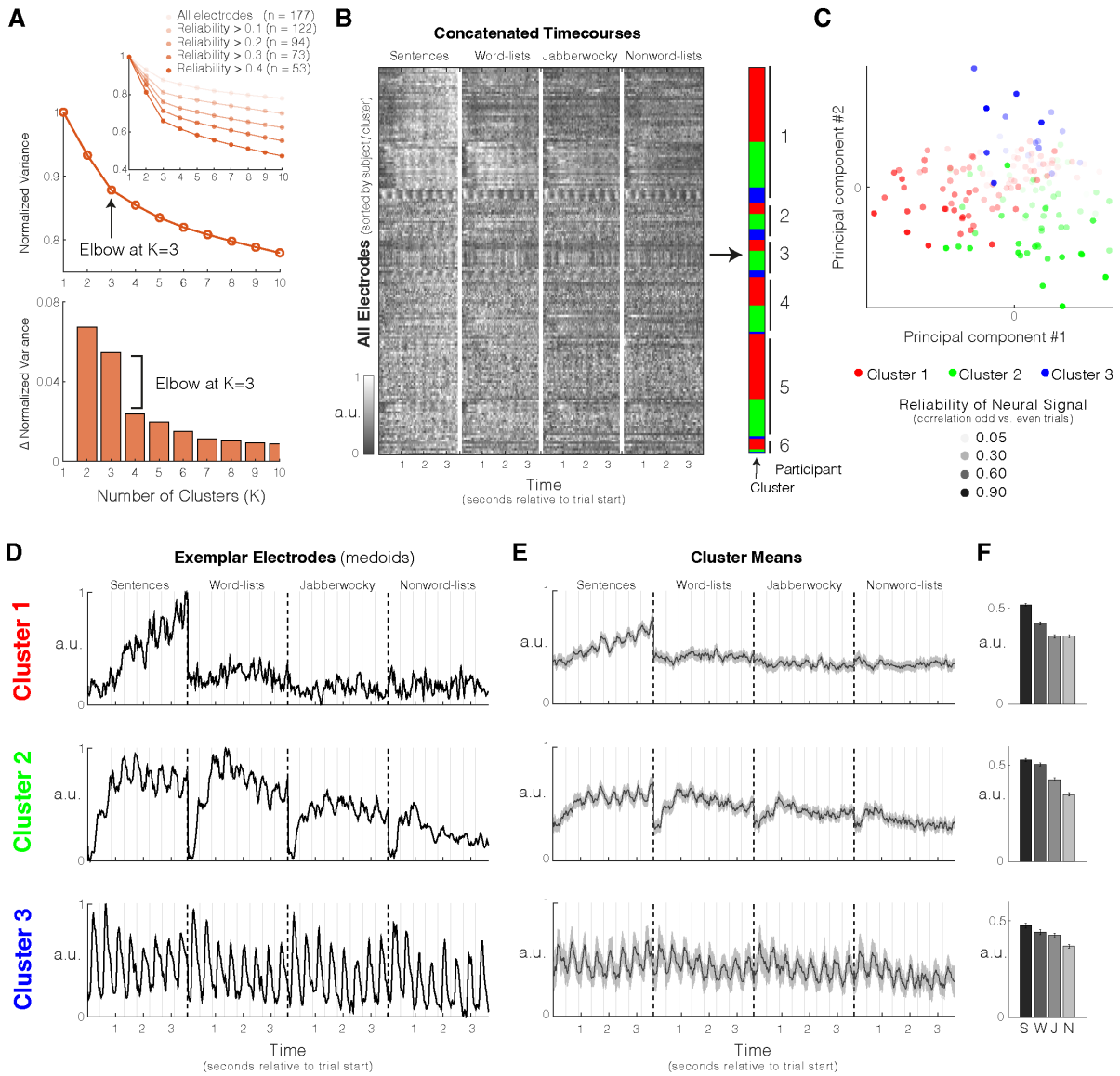

Figure 2 – Dataset 1, k-medoids clustering with k=3. A) Search for optimal k using the "elbow method". **Top:** variance (sum of the distances of all electrodes to their assigned cluster center) normalized by the variance when k=1 as a function of k (normalized variance (NV)). **Inset**: Clustering was performed while omitting electrodes below a parametrically sampled reliability threshold. Orange shading represents the reliability threshold for omitting electrodes. The elbow (point of transition between a steeper to a more moderate slope) gets more pronounced when eliminating lower-reliability electrodes, which strengthens the claim that k=3 best describes these data. **Bottom:** change in NV as a function of k (NV(k+1) – NV(k)). After k=3, there is a large drop in the change in variance, suggesting that 3 clusters appropriately describe this dataset. **B)** Clustering mean electrode responses (concatenated across the four experimental conditions: sentences (S), word-lists (W), Jabberwocky (J), nonword-lists (N)) using k-medoids (k=3) with a correlation-based distance (Methods). Shading of the data matrix reflects normalized high-gamma power (70-150Hz). Electrodes are sorted vertically due to participant and their assignment to clusters (right color bar). All three clusters are present in each of the six participants. **C)** Electrode responses visualized on their first two principal components, colored by cluster and shaded by the reliability of the neural signal as estimated by correlating responses to odd and even trials (**Figure 1D**). **D)** Timecourses of best representative electrodes ('medoids') selected by the algorithm from each of the three clusters. The timecourses reflect normalized high-gamma (70-150Hz) power averaged over all trials of a given condition. a.u. stands for arbitrary units; the signals were

z-scored and normalized to have minimum value of 0 and maximum value of 1. **E)** Timecourses averaged across all electrodes in each cluster. Shaded areas around the signal reflect a 99% confidence interval over electrodes. **F)** Mean condition responses (averaged across all trials) by cluster. Error bars reflect standard error of the mean over electrodes. After averaging across time, response profiles are not as distinct by cluster (especially for Clusters 2 and 3), which underscores the importance of temporal information in elucidating this grouping of electrodes.

We then evaluated the stability of these clusters across trials and their robustness to data loss. We found that clusters derived from half of the data (either odd- or even-numbered trials) are significantly more similar to the clusters derived from the full dataset or from the other half of the data than would be expected by chance (ps<0.001, permutation test, Methods, **Figure 3A**). The clusters are also robust to the number of electrodes used: clustering solutions derived from only a subset of the language-responsive electrodes (down to ~27%, ~32%, and ~69% of electrodes for Clusters 1, 2, and 3, respectively) are significantly more similar to the clusters derived from all the electrodes than would be expected by chance (using a threshold of p<0.05, evaluated with a permutation test, Methods, **Figure 3B**).

To further quantify the apparent differences among the three response profiles, we performed two additional analyses. First, we examined how strongly the neural signal exhibits 'locking' to individual word/nonword onsets by correlating the observed responses with a fitted sinusoidal function (Methods). This analysis revealed that—consistent with visual examination—electrodes in Cluster 3 show the strongest degree of stimulus locking, followed by electrodes in Cluster 2, with electrodes in Cluster 1 showing the weakest stimulus-related time-locking (**Figure 3C**, **Table S1A-B**). And second, we tested how quickly and strongly the S, W, J, and N conditions diverge from one another in each of the profiles. We did this using a binary linear classifier trained for each cluster separately using incrementally more of the timecourse for discrimination (**Figure 3D-F**, Methods). The classification performance (averaged across 10 folds of the cross-validated classifier) revealed that neural populations in Cluster 1 reliably distinguish S from W earlier and more strongly than the neural populations in Clusters 2 and 3. In contrast, neural populations in Cluster 2 reliably distinguish W from N and J from N earlier and more strongly than neural populations in Clusters 1 and 3.

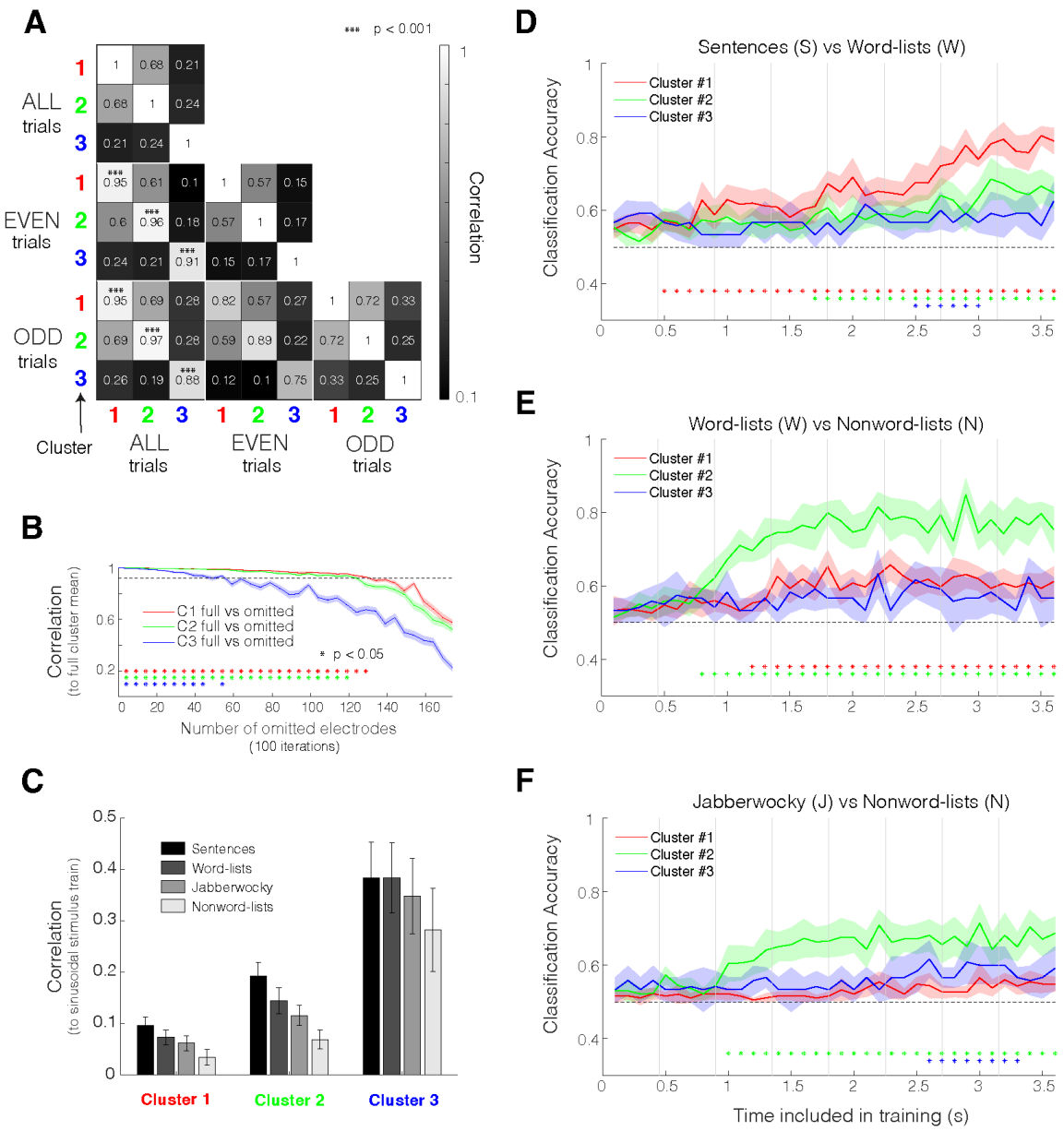

Figure 3 – Evaluation of Dataset 1 clusters. **A)** Comparison of clusters from all trials (top three rows) versus only even (middle three rows) or odd (bottom three rows) trials. Clusters that emerge using only odd or even trials are highly similar to the clusters that emerge when all trials are used and to clusters that emerge when the other half of the data is used (ps<0.001; evaluated with a permutation test; Methods). **B)** Robustness of clusters to electrode omission. Random subsets of electrodes were removed in increments of 5 (Methods). Similarity of cluster centers when all electrodes were used versus when subsets of electrodes were removed. Stars reflect significant similarity with the full dataset (using a threshold of p<0.05; evaluated with a permutation test; Methods). Shaded regions reflect standard error. Cluster 3 is driven the most by individual electrodes relative to Clusters 1 and 2. **C)** Correlation of fitted stimulus train with timecourse of electrodes by cluster and by condition (Methods). Error bars reflect standard error of the mean by electrode. Electrodes in Cluster 3 are the most locked to word/nonword presentation whereas electrodes in Cluster 1 are the least locked to word/nonword presentation. There was a significant main effect for cluster (p<0.05) but not for condition (ANOVA for LME models, Methods, **Table S1A-B**). These qualitative between-condition differences could be due to generally greater engagement of these neural

populations with more language-like stimuli. **D-F)** Classifier performance by cluster as a function of the amount of timecourse included in training (Methods). A binary linear classifier was trained to discriminate sentence (S) and word-list (W) conditions (**D**), word-list (W) and nonword-list (N) conditions (**E**), and Jabberwocky (J) and nonword-list (N) conditions (**F**). Significance stars at the bottom (colored by cluster) reflect discriminability of conditions above chance level (ps<0.05, evaluated as a cluster statistic against a null distribution from permuted labels, Methods). Shaded regions reflect standard error across the 10 folds of the cross-validated classifier.

Although the k-medoids clustering algorithm assigns each electrode to one of k discrete clusters, we wanted to additionally evaluate the degree to which single electrode profiles fall somewhere between the prototypical cluster response profiles. To do this, we computed the partial correlation of every electrode's response profile with that of each of the cluster medoids, while controlling for the other two medoids (**Figure S4,** Methods). This analysis asks how much a particular electrode's correlation with a given cluster medoid can be uniquely attributed to that cluster, as opposed to the other two clusters. If a neural population has a "mixed" response profile, one would expect its partial correlation with another cluster's medoid (when the response profile of its assigned cluster medoid is controlled for) to be high, indicating that the population's response cannot be fully explained by either cluster alone. As shown in **Figure S4B**, this is not the case for most electrodes, suggesting that many of the electrodes exhibit response profiles that are mostly consistent with *one* of the prototypical responses.

Nonetheless, a few electrodes, mostly in Clusters 1 and 2, exhibit high partial correlations with another cluster's medoid (i.e., a "mixed" response profile). Visual inspection of these response profiles (**Figure S4C-D;** osf.io/xfbr8/) reveals that these electrodes exhibit a blend of Cluster 1 and Cluster 2 response characteristics. The existence of mixture electrodes primarily between Clusters 1 and 2 is in line with the generally high correlation between their medoids (0.68 between Cluster 1 and 2 medoids versus 0.21 between Cluster 1 and 3, and 0.24 between Cluster 2 and 3; **Figure 3A**).

2. Response profiles reflect different sizes of temporal receptive windows.

The temporal dynamics of the neural responses across clusters suggested that the observed differences in the response profiles may reflect different 'temporal receptive windows' (TRWs)—a temporal equivalent of spatial receptive fields that corresponds to the amount of the preceding temporal context that affects the processing of the current input (e.g., Hasson et al., 2008, Lerner et al., 2011; Norman-Haignere et al., 2022).

More specifically, the degree to which their responses are 'locked' to individual word/nonwords (**Figure 3C**, Methods), as well as the onset and strength of discriminability between the S, W, J and N conditions (**Figure 3D-F**, Methods) —both described above—point to distinct TRWs. In particular, a neural population that only processes information over the span of a single word should exhibit visible evoked responses at the rate of stimulus presentation, reflecting the momentary stimulus-related fluctuations. On the other hand, a neural population that processes information over spans of multiple words should exhibit a response that reflects a more smoothed version of the stimulus train, with no momentary stimulus-related fluctuations. Indeed, the three clusters differ significantly in their degree of locking to the individual word

onsets. Cluster 3 shows the strongest locking, followed by Cluster 2, with Cluster 1 showing the weakest amount of locking (**Figure 3C**). Moreover, a neural population that only processes information over the span of ~a single word (or less) should show little sensitivity to whether nearby words can be composed into phrases. This is the pattern we see for electrodes in Cluster 3 (**Figure 3D**): these electrodes do not reliably discriminate between the S and W conditions. In contrast, a population that processes information over spans of multiple words should show sensitivity to the composability of nearby words, and thus should strongly discriminate between sentences and word-lists. This is the pattern we see for electrodes in Clusters 1 and 2, with Cluster 1 electrodes showing earlier and stronger discrimination (**Figure 3D**). Note that this greater difference between the Sentence and Word-list conditions for longer-TRW neural populations is presumably due to the fact that linguistic differences between these two conditions become more pronounced for longer strings of words (e.g., see **Figure S5** for evidence from n-gram frequency counts).

To evaluate whether the clusters indeed differ in the size of their TRWs, we constructed a toy model wherein we convolved a simplified stimulus train with response functions of varying widths (TRW sizes denoted as σ; **Figure 4A**, see Methods for model assumptions and implementational details). The resulting simulated responses exhibited striking visual similarity to the observed response patterns (**Figure 4A**). We then computed—for every electrode—a correlation between each simulated response and the observed response, and we selected the σ value that yielded the highest correlation (**Figure 4B-C**, Methods). The estimated TRW sizes showed a clear pattern of decrease from Cluster 1 to 2 to 3; the average σ values per cluster were ~6, ~4, and ~1 words for Clusters 1, 2, and 3, respectively (ps<0.0001 comparing TRWs across all pairs of clusters, evaluated with a LME model, Methods, **Figure 4B-C, Table S5**). To evaluate the robustness of this result, we repeated the TRW fitting procedure using other kernels, and confirmed that the relative sizes of the TRWs of the three clusters did not depend on the specific choice of kernel shape (**Figure S6**). Furthermore, the estimated values of σ in number of words (as reported above) appear to be invariant to the stimulus presentation rate, which suggests that the TRW of language-responsive electrodes is information-, not time-, dependent (**Table S6** and **Table S7**). However, this rate-invariance should be investigated further in future work given the small number of participants in each group (n=3) and, correspondingly, the low statistical power.

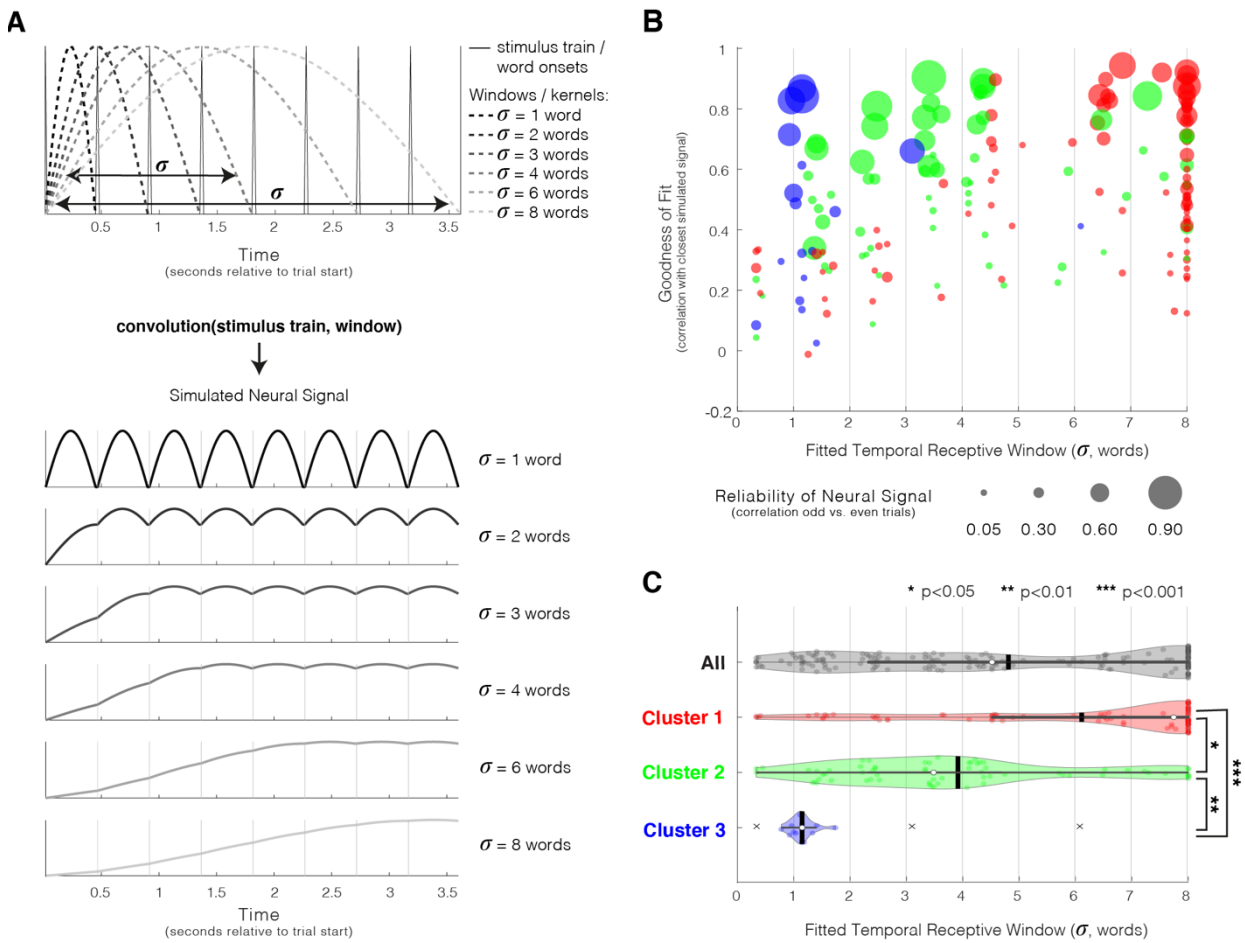

Figure 4 – Estimating the size of the temporal receptive window (TRW) of different electrodes. **A)** A toy model that simulates neural responses to the sentence condition as a convolution of a simplified stimulus train and truncated Gaussian kernels with varying widths. *Top:* Simplified stimulus train where peaks indicate a word/nonword onset, and sample kernels correspond to varying temporal receptive window sizes (σ). The kernels were constructed from Gaussian curves with a standard deviation of $\sigma/2$ truncated at +/- 1 standard deviation (capturing 2/3 of the area under the Gaussian, Methods) and normalized to a minimum of 0 and a maximum of 1. *Bottom:* The resulting simulated neural signals for sample kernel widths, normalized to a minimum of 0 and a maximum of 1. **B)** Best TRW fit for all electrodes colored by cluster and sized by the reliability of the neural signal as estimated by correlating responses to odd and even trials (**Figure 1D**). The goodness of fit, or correlation between the simulated and observed neural signal (Sentence condition only), is shown on the y-axis. **C)** Estimated TRW sizes across all electrodes (grey) and per cluster (red, green, and blue). Black vertical lines correspond to the mean window size and the white dots correspond to the median. "x" marks (present in Cluster 3 only) indicate outliers (more than 1.5 interquartile ranges above the upper quartile or less than 1.5 interquartile ranges below the lower quartile). Significance was evaluated with an LME model (Methods, **Table S5**). Together, B and C show that the clusters vary in the size of their TRWs, from a relatively long TRW (Cluster 1) to a relatively short one (Cluster 3).

3. Clusters 1 and 2 are distributed across the language network, whereas cluster 3 exhibits a posterior bias.

We tested for differences in the anatomical distribution of the electrodes that belong to the 3 clusters in Dataset 1. We excluded from this analysis right-hemisphere (RH) electrodes because only 4 RH electrodes passed the language selectivity criterion (S>N). We focused on the y (posterior-anterior) and z (inferior-superior) directions in the MNI coordinate space within the left hemisphere. Electrodes in both Cluster 1 and 2 were distributed across the temporal and frontal language regions (**Figure 5**). When examining all electrodes together, or focusing on only the frontal or only the temporal electrodes, the MNI coordinates of electrodes in Clusters 1 and 2 did not significantly differ in either of the two tested directions (ps>0.05, evaluated with a LME model, Methods**, Figure 5C-D**, **Table S2A**). However, when weighting the electrodes by their reliability in the LME model, electrodes in Cluster 1 fell more anteriorly and inferiorly relative to electrodes in Cluster 2 (ps<0.05, evaluated with a LME model, Methods, **Table S2B**). Electrodes in Cluster 3 were significantly more posterior than those in Clusters 1 and 2 (lower y-coordinate values, both Clusters 3 vs. 1 and Clusters 3 vs. 2, ps<0.0001, Methods, **Figure 5C, Table S2A**).

To complement this analysis, we visualized the anatomical distribution of electrodes in two additional ways. First, we visualized all language-responsive electrodes by their partial correlations to each of the cluster medoids (**Figure S4E**). This approach does not enforce a categorical grouping into clusters, potentially allowing us to see more subtle response gradients. However, this analysis revealed a similar picture: Cluster-1- and Cluster-2-like responses are present throughout frontal and temporal areas, whereas Cluster-3-like responses are localized to the posterior superior temporal gyrus. Second, we examined the distribution of electrodes by their fitted TRW (**Figure 5F**). This visualization exhibits a gross anatomical trend of TRWs increasing from posterior to anterior regions, however, there remains a substantial local mosaic pattern, with some long-TRW electrodes present in posterior temporal areas and some short-TRW electrodes present in anterior temporal and frontal areas.

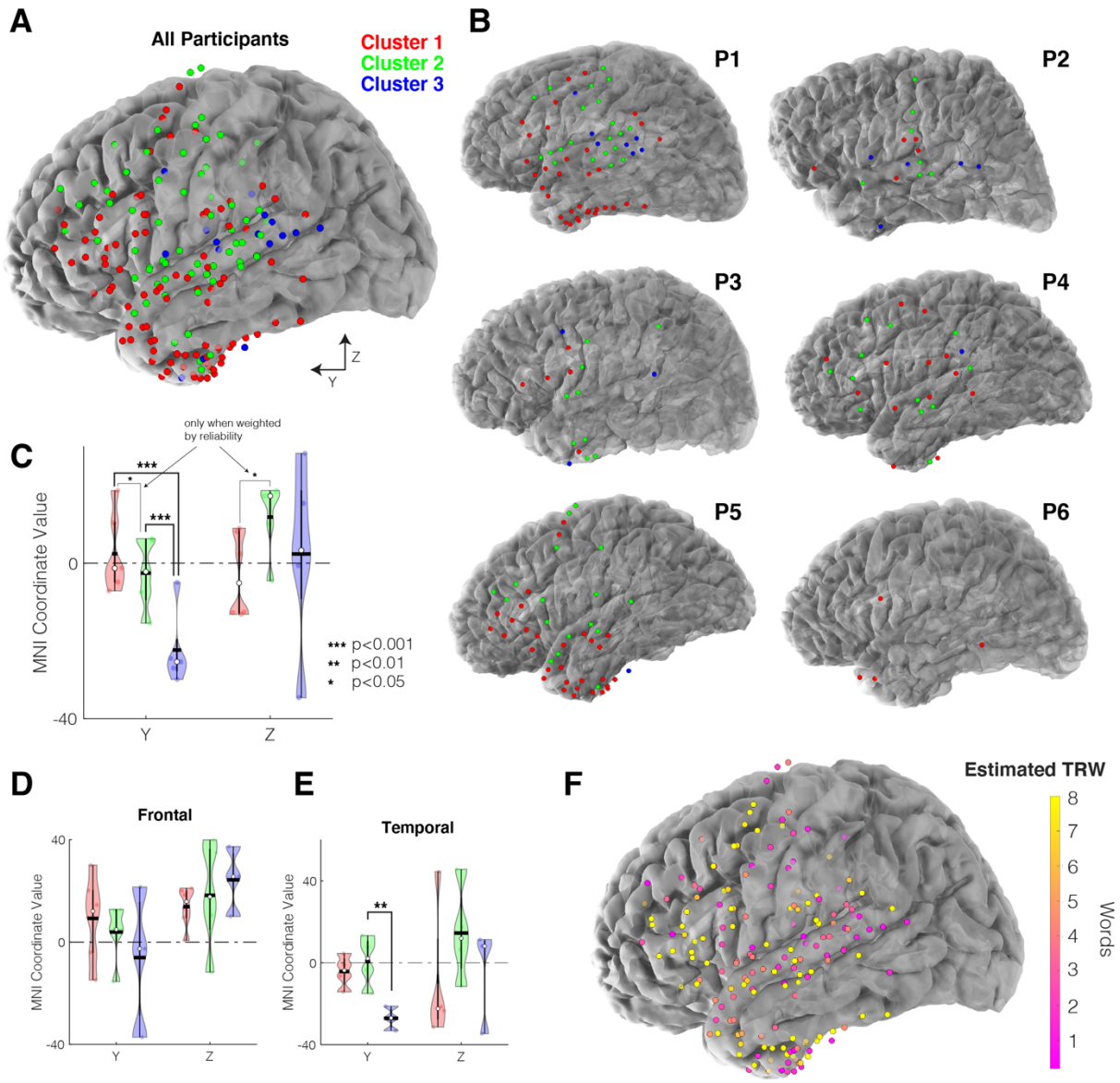

Figure 5 – Anatomical distribution of the clusters in Dataset 1. A) Anatomical distribution of language-responsive electrodes in Dataset 1 across all participants in MNI space, colored by cluster. **B)** Anatomical distribution of language-responsive electrodes in participant-specific space. **C-E)** Violin plots of MNI coordinate values for the 3 Clusters, where plotted points represent the mean of all coordinate values for a given participant and cluster. The mean across participants is plotted with a black horizontal line, and the median is shown with a white circle. Significance was evaluated with a LME model (Methods). Cluster 3 exhibits a posterior bias (more negative Y coordinate) relative to Cluster 1 and 2 when modeled using all language electrodes (ps<0.001, **C**)**.** This trend is also evident when examining only the frontal (**D**) or temporal electrodes separately, but the difference only reaches significance for the temporal electrodes (p<0.01, E). **F)** Anatomical distribution of electrodes in Dataset 1 colored by their estimated temporal receptive window (TRW, **Figure 4**). There is a slight trend of increasing TRW size from posterior to anterior regions, but considerable local heterogeneity exists.

4. Clusters 1 and 3 replicate in Dataset 2 and Cluster 2 partly replicates.

We asked whether the same clusters would emerge in a second, independent dataset with new participants and different linguistic materials (Dataset 2; 16 participants; 362 language-responsive electrodes; mostly depth electrodes, **Figure 6A**, Methods). Participants in Dataset 2 only saw two of the four conditions presented to participants in Dataset 1 (Sentences (S) and Nonword-lists (N), but not Word-lists (W) or Jabberwocky sentences (J)); therefore, we started by re-clustering the electrodes from Dataset 1 using only the responses to the S and N conditions to allow for direct comparisons with Dataset 2.

The cluster centers when only the S and N conditions were used exhibited a strong qualitative similarity to those of the clusters derived using the data from all four conditions (**Figure S7**), and ~80% of electrodes in Dataset 1 were assigned to the same cluster ('matched' to the original clusters by highest correlation). However, Cluster 2 was now less robust to electrode loss than Clusters 1 and 3 (compare the green curve in **Figure 3B** to the green curve in **Figure S7G**). This suggests that responses to the Word-list and Jabberwocky conditions may be especially important for differentiating Cluster 2 from the other response profiles, presumably because these conditions pattern differently for Clusters 1 and 2.

We next clustered the electrodes in Dataset 2 using the same approach as for Dataset 1. The optimal number of clusters in Dataset 2 was k=2 based on the elbow method, and the resulting clusters were visually similar to Clusters 1 and 3 from Dataset 1 ($p<0.001$ for Cluster 3, $p=0.061$ for Cluster 1, permutation test, Methods, osf.io/xfbr8/. Note that our permutation test is especially conservative when there are only two experimental conditions and when k=2). To test whether Cluster 2 could emerge from Dataset 2, we also clustered Dataset 2 enforcing k=3 (**Figure 6**). When the electrodes in Dataset 2 were clustered into three groups, the same two cluster centers as in the case of k=2 were again apparent and showed reliable similarity to Clusters 1 and 3 in Dataset 1 ($p<0.001$ and $p=0.023$, respectively, permutation test, Methods, **Figure 6G, I**). The third cluster qualitatively resembled Cluster 2 from Dataset 1 (**Figure 6G**), but the resemblance was not statistically reliable ($p=0.732$).

As another, less stringent, test of whether Cluster 2 responses were present in Dataset 2, we assigned each electrode in Dataset 2 to a cluster from Dataset 1 based on their highest correlation with the average response profiles (**Figure S8**). Following this procedure, a substantial number of electrodes (n=95 of the total of n=177) were assigned to Cluster 2, and the response profile of this group of electrodes was reliably similar to Cluster 2 profile from Dataset 1 ($p=0.001$, permutation test, Methods). This analysis indicates that Cluster-2-like responses were indeed present in Dataset 2, even though they did not reliably emerge as a dominant response profile through the data-driven clustering approach. The lower robustness of the Cluster 2 response in Dataset 2 may be, in part, attributable to the lower data quality of Dataset 2 compared to Dataset 1 (compare **Figure 6B** vs. **6C**), as well as the sparser surface coverage due to the prevalence of depth electrodes (**Figure 6A**). For completeness, an analysis of the anatomical trends in Dataset 2 are presented in **Figure S9** (**Tables S3** and **S4**).

Finally, we estimated the temporal receptive window (TRW) size (as in Section 2 above) for each electrode in Dataset 2 (**Figure S10**). Clusters 1 and 3 (the two clusters that consistently replicated from Dataset 1), were best described by TRWs of ~4.5 and ~1 words, respectively (**Figure S10A, B**), similar to the TRW sizes observed for those clusters in Dataset 1. The TRW of Cluster 2 did not significantly differ from Cluster 3 when relying on the electrode assignments from the clustering algorithm with k=3 (where Cluster 2 did not replicate, Methods, **Figure 6**, **Figure S10B**, **Table S8**). However, when assigning electrodes by their correlation to the Dataset 1 clusters (where Cluster 2 *did* replicate, **Figure S8**, **Figure S10D**), the TRW of Cluster 2 significantly differed from that of Cluster 3 and was similar to the TRW of Cluster 2 in Dataset 1; ~2.1 words (ps<0.001 comparing TRWs across all pairs of clusters, evaluated using an LME model, Methods, **Figure S10C-D, Table S9**).

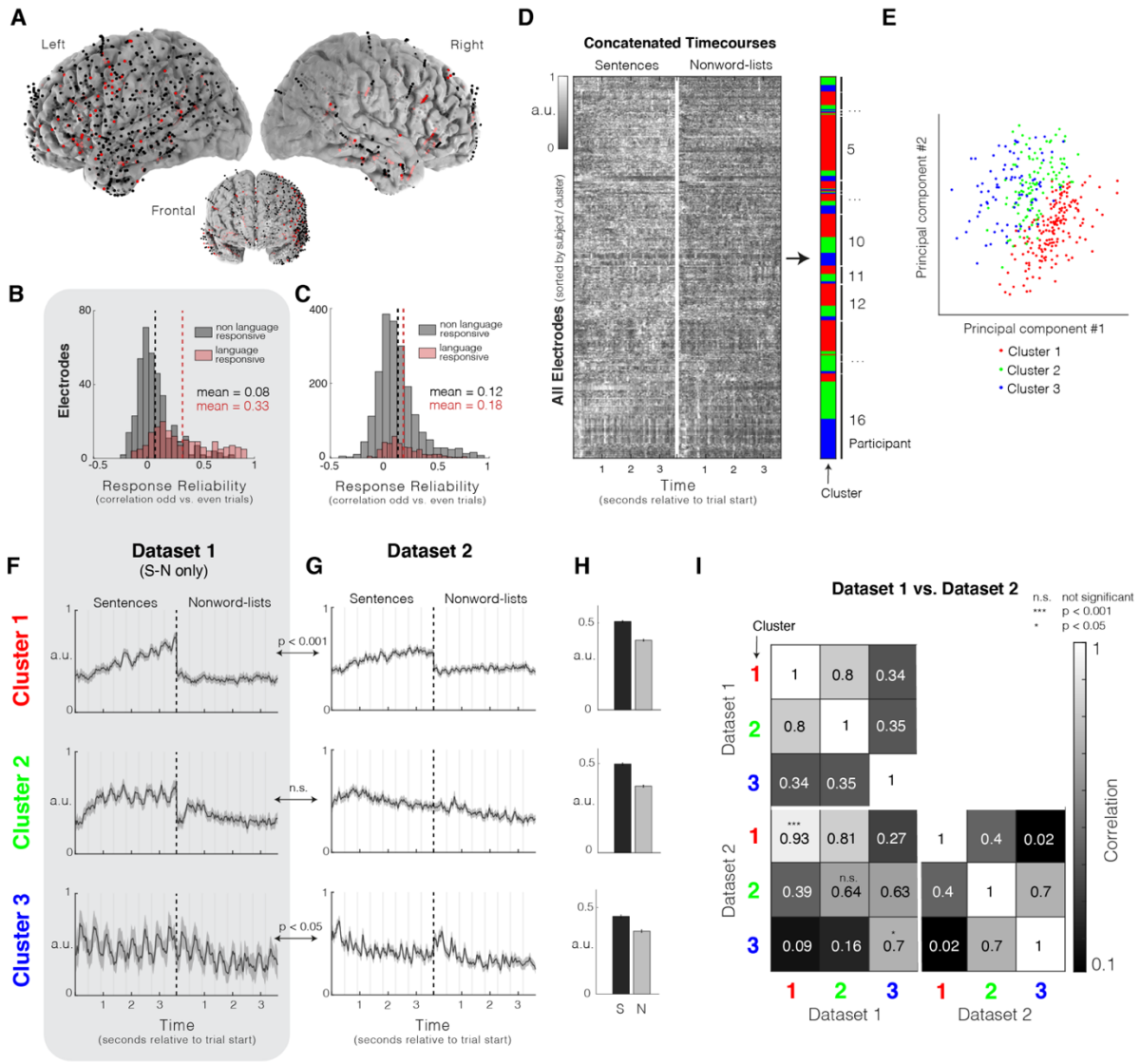

Figure 6 – Dataset 2 k-medoids clustering with k=3. A) The locations of language-responsive (n=362, red; Methods) and non-language-responsive (n=2,017, black) electrodes across the sixteen participants in Dataset 2 (both

surface and depth electrodes were implanted). Language-responsive electrodes were found across the cortex, in both the left and right hemispheres (**Table 2**). **B and C)** Response reliability as estimated by correlating responses to odd and even trials for language-responsive and non-language-responsive electrodes (as in **Figure 1D**). Language-responsive electrodes exhibit more reliable responses to linguistic stimuli than non-language-responsive electrodes for both Dataset 1 (S+N conditions only, B) and Dataset 2 (C), however, the responses of language electrodes are less reliable in Dataset 2 than Dataset 1. **D)** Clustering mean electrode responses (S+N) in Dataset 2 using k-medoids (k=3) with a correlation-based distance. Shading of the data matrix reflects normalized high-gamma power (70-150Hz). **E)** Electrodes visualized on their first two principal components, colored by cluster. **F and G)** Average timecourse by cluster from Dataset 1 when using only S and N conditions (**F**; see **Figure S7**) and from Dataset 2 (**G**). Shaded areas around the signal reflect a 99% confidence interval over electrodes. **H)** Mean condition responses by cluster in Dataset 2. Error bars reflect standard error of the mean over electrodes. Again, after averaging across time, response profiles are not as distinct by cluster, underscoring the importance of temporal information in elucidating this grouping of electrodes. **I)** Evaluation of clusters from Dataset 1 (clustering with S and N conditions only) against clusters from Dataset 2. Clusters 1 and 3 from Dataset 1 replicate to Dataset 2 ($p<0.001$ and $p=0.023$, respectively; permutation test; Methods), and although Cluster 2 demonstrates some qualitative similarity across the two datasets, this similarity is not statistically reliable ($p=0.732$, permutation test, Methods).

Discussion

The nature of the neural computations that support our ability to extract meaning from linguistic input remains an important open question in the field of language research. Here, we leveraged the high temporal and spatial resolution of human intracranial recordings to probe the fine temporal dynamics and the spatial distribution of language-responsive electrode locations. We uncovered three temporal profiles of response during the processing of sentences and linguistically degraded conditions such as lists of words or nonwords. We suggest that these profiles differ in the size of their temporal receptive window (TRW)—the amount of temporal context that affects the neural processing of the current input. Further, we found that electrodes with distinct response profiles manifest in a scattered distribution across both frontal and temporal cortices. Below, we contextualize these results with respect to prior empirical work and discuss their implications for our understanding of human language processing.

Three profiles characterize language-responsive neural populations

In the present study, we used a clustering approach in order to group neural populations (as measured by intracranial macroelectrodes, note that when we write that '*electrodes'* exhibit a response, we are referring to the *neural populations* that the electrodes are measuring) by their responses to four types of language stimuli: sentences (S), lists of unconnected words (W), Jabberwocky sentences (where content words are replaced with pronounceable nonwords; J), and lists of nonwords (N). We uncovered three dominant response profiles ('clusters') that differed in the presence and timing of the increase (build-up) of neural activity over the course of a sentence, the degree of locking to individual word/nonword onsets, and the overall magnitude of response to the linguistically degraded conditions (W, J, and N). Within each cluster, individual electrodes exhibited highly similar responses, with a small number of electrodes displaying a mixed response between Clusters 1 and 2. Finally, we found evidence for each of the three response profiles in an independent dataset that only included two of the four linguistic conditions (sentences and nonword-lists), although Clusters 1 and 3 were more robustly replicable. Importantly, because we had restricted our analyses to electrodes that show a functional signature of the language network (a stronger overall response during the processing of structured and meaningful language stimuli—sentences—than during the processing of perceptually similar but meaningless and unstructured stimuli—nonword-lists; Fedorenko et al., 2010), these findings provide evidence for ***functional heterogeneity within the language network*** proper, rather than between the language areas and nearby functionally distinct brain regions, like speech areas (e.g., Overath et al., 2015; Keshishian et al., 2023) or higher-level cognitive networks (e.g., Braga et al., 2020; Fedorenko & Blank 2020; Shain, Paunov, Chen et al., 2022c).

The experimental design adopted in the current study has traditionally been used as a way to tease apart neural responses to word meanings (present in S and W, but not in J and N) and syntactic structure (present in S and, under some views of syntax, in J, but not in W/N; Fedorenko et al., 2010, 2012, 2016; for earlier uses of this paradigm, see Mazoyer et al., 1993; Friederici et al., 2000; Humphries et al., 2001; Vandenberghe et al., 2002). As measured with fMRI, all areas

of the language network show a profile that suggests sensitivity to both word meanings and syntactic structure: the response is strongest to S, lower to W and J, and lowest to N (e.g., Fedorenko et al., 2010; Bedny et al., 2011; Shain, Kean et al., 2023; Pallier et al., 2011; Desbordes et al., 2023 see Bautista & Wilson, 2016 and Fedorenko et al., 2020 for evidence against the lexical/syntactic dissociation from other paradigms; see Dick et al., 2001 for earlier arguments and evidence). Using a similar design in an intracranial recording study, Fedorenko et al. (2016) replicated this overall pattern of response, while additionally revealing its coarse temporal dynamics. More specifically, Fedorenko et al. (2016) reported a temporal profile—present in a subset of electrodes—whereby high gamma power response builds-up over the course of a sentence but not in other conditions (replicated by Nelson et al., 2017; Desbordes et al., 2023; Woolnough et al., 2023), which they interpreted as indexing the process of constructing a sentence-level meaning. Here, we investigated the temporal profiles of language-responsive electrodes more comprehensively. By leveraging the fine-grained temporal information in the signal (i.e., considering the full timecourses instead of averaging high gamma power in each word/nonword as in Fedorenko et al., 2016), we found that the build-up neural populations reported in Fedorenko et al. (2016) represent a mix of functionally distinct populations. The timecourse of response to the S condition in Fedorenko et al. (2016) is most similar to that in Cluster 1 here. However, the fact that in Fedorenko et al. (2016) a reliable S>W>J>N profile was present suggests a contribution from Cluster 2 neural populations. As such, our analyses identify two functionally distinct build-up profiles and additionally uncover a third profile, which does not show build-up of activity over time, and we replicated these results in a new, larger dataset with a different set of language materials (Dataset 2). Importantly, here we show that in spite of strong integration between lexical and syntactic processing, neural populations within the language network *do* differ functionally, although along a different dimension—the temporal scale of information integration.

The response profiles reflect distinct temporal receptive windows

A temporal receptive window (TRW) denotes the amount of the preceding context that a given neural unit integrates over (e.g., Hasson et al., 2008; Lerner et al., 2011; Norman-Haignere et al., 2022). Previous studies have demonstrated that cortical neural activity is organized into a hierarchy of timescales, wherein information over tens to hundreds of milliseconds is encoded by sensory cortical areas, and information over many seconds is encoded by higher order areas (Chaudhuri et al., 2015; Runyan et al., 2017; Murray et al., 2014; Chien et al., 2020). Past fMRI studies have shown that the TRW of the language network falls somewhere between a word and a short clause/sentence (e.g., Lerner et al., 2011; Jacoby and Fedorenko, 2020; Blank and Fedorenko, 2020; Jain et al., 2020; Caucheteux et al., 2023; Chang et al., 2022), although some work has suggested that language regions are, at least to some degree, sensitive to sub-lexical regularities (Bozic et al., 2010; Regev et al., 2021). Using a simple instantiation of an information processing system—with one (interpretable) free parameter: the length of past stimulus context—we estimated the TRW of individual language-responsive neural populations. Based on this analysis, we argue that our observed ***response profiles differ in their timescale of information processing***, from sub-lexical units and single words (Cluster 3) to short phrases (Cluster 2) to longer phrases/sentences (Cluster 1).

Do the observed response profiles reflect categorically distinct clusters that integrate information over different timescales, or is the underlying structure of language-selective responses in the brain best described by a continuum of TRWs with no sharp boundaries or groupings of response types? Although we do not rule out the possibility of a TRW continuum, our data are well explained by the grouping of responses into **three** categories. Although some electrodes do exhibit a "mixed" response profile, falling somewhere between the prototypical Cluster 1 and Cluster 2 responses, this mixing could be due to these electrodes picking up activity of multiple neural populations. Recordings at a higher spatial resolution would be needed to evaluate this possibility (e.g., Paulk et al., 2022; Leonard, Gwilliams et al., 2023). Nevertheless, the current data suggests the existence of neural populations within the language network that are sensitive to information chunks of *distinct and specific size.* This functional organization is presumably driven by the statistics of natural language and is likely critical for efficient extraction of meaning from language.

To estimate the TRW values, we made several simplifying assumptions that can be revisited in future studies. First, we have discussed TRWs in terms of the number of *words*. However, natural languages vary substantially in how they package information into words (Evans & Levinson, 2009) and the processing of a given word is highly dependent on how informative the word is in context (e.g., Shannon, 1949; for behavioral evidence, see Levy, 2008; Shain et al., 2022b). As a result, TRWs may instead be bounded by the number of bits of information. Future work should evaluate multiple accounts of the units in which TRWs are measured. The second simplifying assumption is that TRWs are *fixed* in size. Much recent evidence suggests that human comprehension mechanisms can flexibly accommodate corrupt linguistic input, e.g., due to speech errors (e.g., Levy, 2008; Gibson et al., 2013; Gibson et al., 2017; Keshev & Meltzer-Asscher, 2021; Ryskin et al., 2018, 2021; see Gibson et al., 2019 for a review), which may make it desirable for TRWs to be somewhat adaptable to allow for the possibility of continuously revising one's interpretation of incoming input. Future work should seek to understand if and how the TRW of a specific neural population can be affected by linguistic context. And third, the response function (kernel) that we used to generate the simulated signals was overly simplified and is likely not consistent with the underlying neurophysiology (see Methods for details). A model that is more faithful to neurobiological principles may better capture the observed neural responses and such models should be explored in future work. We thus acknowledge that our toy model is simplistic, but we wanted to estimate TRW sizes in an objective manner with the fewest possible assumptions.

Finally, our TRW modeling does not currently incorporate any linguistic processing of the incoming stimulus and we therefore can only capture a neural population's average response to the Sentence condition. However, we suggest that the TRW framework can be extended to incorporate processing of specific linguistic content. In particular, neural populations in the language network should not only be sensitive to different lengths of past context, but their response should also scale with how well the stimulus matches natural language statistics (Tuckute et al., 2023) *at the relevant context length*. The TRW's "gating" of linguistic input into different lengths of 'effective' input (which our model captures), followed by scaling of the neural

response by the effective input's probability/plausibility, evaluated against past linguistic experience (which our model does not capture), may explain the better discriminability between the Sentence and Word-list conditions by Cluster 1 populations which track long contexts. Incorporating linguistic probability/plausibility into the model would move us closer to a stimulus-dependent account of linguistic computations carried out by the language network and can be evaluated in future experiments by manipulating linguistic probability/plausibility of n-grams at varying scales.

The distributed nature of language processing

There is a long history in language neuroscience seeking to divide the process of language comprehension into both temporally distinct stages and spatially distinct components. At some level, this kind of architecture indeed characterizes language processing. In particular, clear separation exists between the language-processing system (Fedorenko et al., 2011) and both i) lower-level perceptual areas, like the speech-perception areas (Norman-Haignere et al., 2015; Overath et al., 2015; Keshishian et al. 2023) and the visual word-form area (e.g., Baker et al., 2007; Hamamé et al., 2013; Saygin et al., 2016) and ii) putative higher-level cognitive areas (like the Default network; Buckner & DiNicola, 2019; or the Theory of Mind network; Saxe et al., 2006) that may carry out further processing on the meaning representations extracted from language (e.g., Lerner et al., 2011; Baldassano et al., 2017; 2018). However, finding spatial sub-divisions *within* the language-selective network has proven challenging (e.g., Fedorenko et al., 2010, 2020; Bautista & Wilson, 2016).

The current work demonstrates that although there exist functional differences within the language network, these functionally distinct mechanisms are generally *not spatially clustered* and are instead distributed in an interleaved fashion across the language network. The latter explains why most past fMRI work could not reveal this functional heterogeneity (cf. Fedorenko et al., 2012 for implied functional heterogeneity given the information present in multivariate patterns of fMRI response; and see Jain et al., 2020 for evidence of voxel-level heterogeneity with respect to TRWs as discovered in an encoding approach with artificial neural network (ANN) language models). A clear exception in our data is the concentration of Cluster 3 (shortest-TRW) electrodes in the posterior superior temporal gyrus, which may suggest that this area serves a unique computational role within the language network, and/or that these electrodes are picking up some activity from the nearby speech areas (e.g., Overath et al., 2015).

Future directions

The current findings lay the foundation for several exciting future research avenues. First, the size of a neural unit's temporal receptive window (TRW) should determine its sensitivity to different linguistic features. One limitation of the current investigation is the focus on condition-level differences, rather than trying to explain fine-grained responses to individual linguistic items. The reason for this choice is two-fold. First, the current linguistic materials were not constructed with the goal of investigating linguistic (e.g., lexical and syntactic) features: in order

to make the materials easy to process for diverse populations, the sentences were constructed to be short and to use common structures and words, which limits the range of variability to be explored. And second, we did not observe reliable stimulus-related activity (beyond the level of conditions; osf.io/xfbr8/). The TRW-based framework makes clear predictions that can be evaluated in future work. For example, short-TRW populations should show greater sensitivity to lexical features, such as word frequencies, whereas longer-TRW populations should be more sensitive to linguistic features at longer timescales, such as higher-order n-gram frequencies and syntactic-structure-related features. However, because many linguistic features are strongly inter-correlated in naturalistic language materials (e.g., Piantadosi et al., 2011; Shain, Blank et al., 2020; Shain et al., 2022; see osf.io/xfbr8/ for evidence of inter-correlation of linguistic features in the current stimuli), evaluating these predictions will require constructing materials that are specifically designed to best dissociate different linguistic dimensions.

Second, artificial neural network (ANN) language models—which have proven to be powerful tools for understanding the human language system (Toneva & Wehbe, 2019; Jain et al., 2020; Schrimpf et al., 2021; Goldstein et al., 2022; Caucheteux & King, 2022)—could be leveraged to gain insights into the constraints on language processing architecture. For example, do successful language architectures require particular proportions of units with different TRWs or particular distributions of such units within and/or across model layers? In Dataset 1, we found the fewest electrodes belonging to Cluster 3 (shortest TRW), more electrodes belonging to Cluster 2 (intermediate TRW), and the majority of electrodes belonging to Cluster 1 (longest TRW). These proportions align with the idea that compositional semantic space is highly multi-dimensional, but word-form information can be represented in a relatively low-dimensional space (e.g., Mollica and Piantadosi, 2019). However, the proportions can also be affected by biases in where intracranial electrodes tend to be implanted, so investigating these questions in ANNs, where we can probe all units in the network and have the freedom to alter the architecture in various ways, may yield insights that cannot be gained from human brains at least with the current experimental tools available.

And third, we have here focused on language *comprehension.* However, the same language network also supports language production (Awad et al., 2007; Menenti et al. 2011; Segaert et al. 2012; Silbert et al., 2014; Giglio et al., 2022; Hu, Small et al.,2022). Whether the TRW-based organization discovered here in a language comprehension task applies to language production—given that utterance planning is known to unfold at multiple scales (e.g., Lee et al., 2013)—remains to be determined.

In conclusion, across two intracranial-recording datasets, we here demonstrate the existence of functionally distinct neural populations within the fronto-temporal language-selective network proper, opening the door to investigations of how these populations work together to accomplish the incredible feats of language comprehension and production.

Methods

Participants

Dataset 1 (also used in Fedorenko et al., 2016)*:* Electrophysiological data were recorded from intracranial electrodes in 6 participants (5 female, aged 18–29 years) with intractable epilepsy. These participants underwent temporary implantation of subdural electrode arrays at Albany Medical Center to localize the epileptogenic zones and to delineate it from eloquent cortical areas before brain resection. All participants gave informed written consent to participate in the study, which was approved by the Institutional Review Board of Albany Medical Center. One further participant was tested but excluded from analyses because of difficulties in performing the task (i.e., pressing multiple keys, looking away from the screen) during the first five runs. After the first five runs, the participant required a long break during which a seizure occurred.

Dataset 2: Electrophysiological data were recorded from intracranial electrodes in 16 participants (4 female, aged 21-66 years) with intractable epilepsy. These participants underwent temporary implantation of subdural electrode arrays and depth electrodes to localize the epileptogenic zones before brain resection at one of four sites: Albany Medical Center (AMC), Barnes-Jewish Hospital (BJH), Mayo Clinic Jacksonville (MCJ), and St. Louis Children's Hospital (SLCH). All participants gave informed written consent to participate in the study, which was approved by the Institutional Review Board at each relevant site. Two further participants were tested but excluded from analyses due to the lack of any language-responsive electrodes (see Language-Responsive Electrode Selection).

Data Collection

Dataset 1: The implanted electrode grids consisted of platinum-iridium electrodes that were 4 mm in diameter (2.3–3 mm exposed) and spaced with an inter-electrode distance of 0.6 or 1 cm. The total numbers of implanted grid/strip electrodes were 120, 128, 98, 134, 98, and 36 for the six participants, respectively (**Table 1**). Electrodes were implanted in the left hemisphere for all participants except P6, who had bilateral coverage (16 left hemisphere electrodes). Signals were digitized at 1,200 Hz.

Dataset 2: The implanted electrode grids and depth electrodes consisted of platinum-iridium electrodes. Implanted grid contacts were spaced at 0.6 or 1cm (2.3–3 mm exposed), while SEEG leads were spaced 3.5 - 5 mm depending on the trajectory length, with 2 mm exposed. The total numbers of implanted electrodes by participant can be found in **Table 2** (average=167 electrodes; st. dev.=51; range 92-234), along with the frequencies at which the signals were digitized. Electrodes were implanted in only the left hemisphere for 2 participants, in only the right hemisphere for 2 participants, and bilaterally for 12 participants (**Table 2**). All participants, regardless of the lateralization of their coverage, were included in all analyses.

For both datasets, recordings were synchronized with stimulus presentation and stored using the BCI2000 software platform (Schalk et al., 2004).

Cortical Mapping

Electrode locations were obtained from post-implantation computerized tomography (CT) imaging and co-registered with the 3D surface model of each participant's cortex—created from the preoperative anatomical MRI image—using the VERA software suite (Adamek et al., 2022). Electrode locations were then transformed to MNI space within VERA via nonlinear co-registration of the subjects' skull-stripped anatomical scan and the skull-stripped MNI152 Freesurfer template using ANTs (Avants et al., 2008).

Preprocessing and Extraction of Signal Envelope

Neural recordings were collected and saved in separate data files by run (see Experiment and **Tables 1-2**), and all preprocessing procedures were applied *within* data files to avoid inducing artifacts around recording breaks.

First, the ECoG/sEEG recordings were high-pass filtered at the frequency of 0.5 Hz, and line noise was removed using IIR notch filters at 60, 120, 180, and 240 Hz. The following electrodes were excluded from analysis: a) ground, b) reference, and c) those that were not ECoG or sEEG contacts (e.g., microphone electrodes, trigger electrodes, scalp electroencephalography (EEG) electrodes, EKG electrodes), as well as d) those with significant line noise, defined as electrodes with line noise greater than 5 standard deviations above other electrodes, e) those with large artifacts identified through visual inspection, and, for all but four participants, f) those that had a significant number of interictal discharges identified using an automated procedure (Janca et al., 2015). (For 4 participants—P3 in Dataset 1 and P15, P17, and P21 in Dataset 2—electrodes that were identified as having a significant number of interictal discharges were not excluded from analyses because more than 1/3 of each of these participants' electrodes fit this criterion.) These exclusion criteria left 108, 115, 92, 106, 93, and 36 electrodes for analysis for the 6 participants in Dataset 1 (**Table 1**) and between 76 and 228 electrodes for the 16 participants in Dataset 2 (**Table 2**).

Next, the common average reference (from all electrodes connected to the same amplifier) was removed for each timepoint separately. The signal in the high gamma frequency band (70 Hz–150 Hz) was then extracted by taking the absolute value of the Hilbert transform of the signal extracted from 8 gaussian filters (center frequencies: 73, 79.5, 87.8, 96.9, 107, 118.1, 130.4, and 144; standard deviations (std): 4.68, 4.92, 5.17, 5.43, 5.7, 5.99, 6.3, and 6.62, respectively, as in e.g., Dichter et al., 2018). The resulting envelopes from each of the Gaussian filters were averaged into one high gamma envelope. We focus on the high gamma frequency range because this component of the signal has been shown to track neural activity most closely (e.g., Janca et al., 2015). Linear interpolation was used to remove data points whose magnitude was more than 5 times the 90th percentile of all magnitudes (Norman-Haignere et al., 2022), and we downsampled the signal by a factor of 4. For all data analysis basic Matlab (version 2021a) functions were used.

Finally, the data were z-scored and normalized to a min/max value of 0/1 to allow for comparisons across electrodes, and the signal was downsampled further to 60 Hz (regardless of the participant's native sampling frequency) to reduce noise and standardize the sampling frequency across participants. For the participants who performed a slower version of the

paradigm (e.g., words presented for 700 ms each; see Experiment), the signal was time-warped to a faster rate (words presented for 450 ms each) so that timecourses could be compared across subjects. This time-warping was done by resampling (Matlab procedure *resample*).

Experiment

Dataset 1: In an event-related design, participants read sentences, lists of words, Jabberwocky sentences, and lists of nonwords. All stimuli were eight words/nonwords long. The materials were adapted from Fedorenko et al. (2010; Experiment 2) and the full details of stimulus construction are described there. In short, sentences were manually constructed to cover a wide range of topics using various syntactic structures. Sentences were intended to be easily read, to fit participants with diverse clinical conditions and only included mono- and bi-syllabic words.
The full list of materials is available at OSF (https://osf.io/xfbr8/). The word-lists were created by scrambling the words from the sentences. Jabberwocky sentences were created from the sentences by removing content words (e.g., nouns, verbs, etc.), but leaving the syntactic frame, consisting of function words (e.g., articles, conjunctions, prepositions, pronouns, etc.), intact. Content words were replaced with other pronounceable nonwords, matched for length (in syllables). Lastly, the nonword-lists were generated from scrambling the words/nonwords from the Jabberwocky condition. Originally, a set of 160 items per each condition were created and here, 80 or 60 items of those were used (depending on stimulus presentation rate, as detailed below).

Each event (trial) consisted of eight words/nonwords, presented one at a time at the center of the screen. At the end of each sequence, a memory probe was presented (a word in the sentence and word-list conditions, and a nonword in the Jabberwocky and nonword-list conditions) and participants had to decide whether the probe appeared in the preceding sequence by pressing one of two buttons. Two different presentation rates were used: P1, P5, and P6 viewed each word/nonword for 450 ms (fast-timing), and P2, P3, and P4 viewed each word/nonword for 700 ms (slow-timing). The presentation speed was determined before the experiment based on the participant's preference. After the last word/nonword in the sequence, a fixation cross was presented for 250 ms, followed by the probe item (1,400-ms fast-timing, 1,900 ms slow-timing), and a post-probe fixation (250 ms). Behavioral responses were continually recorded, but only responses 1 second before and 2 seconds after the probe were considered for calculating behavioral performance (**Table 3**). Participants performed best on the sentence trials and worst on the nonword-list trials, with an average accuracy across all conditions of 81.01% (**Table 3**). After each trial, a fixation cross was presented for a variable amount of time, semi-randomly selected from a range of durations from 0 to 11,000 ms, to obtain a low-level baseline for neural activity.

Trials were grouped into runs to give participants short breaks throughout the experiment. In the fast-timing version of the experiment, each run included eight trials per condition and lasted 220 s, and in the slow-timing version, each run included six trials per condition and lasted 264 s. The total amount of intertrial fixation in each run was 44 s for the fast-timing version and 72 s for the slow-timing version. All participants completed 10 runs of the experiment, for a total of 80 trials per condition in the fast-timing version and 60 trials per condition in the slow-timing version.

Dataset 2: In an event-related design that was similar to the one used in Dataset 1, participants read sentences and lists of nonwords (the other two conditions—lists of words and Jabberwocky sentences—were not included). The materials were adapted from a version of the language localizer in use in the Fedorenko lab (e.g., Lipkin et al., 2022). The sentences came from a language corpus (Brown corpus; Kučera et al., 1967) where we searched for 12-word long sentences and chose a diverse set among those. The nonwords were created using the Wuggy software to match to the words from the sentences on low-level phonology.

Each event (trial) consisted of twelve words/nonwords, presented one at a time at the center of the screen. At the end of each sequence, a memory probe was presented (a word in the sentence condition and a nonword in the nonword-list condition) and participants had to decide whether the probe appeared in the preceding sequence by pressing one of two buttons. Two presentation rates were used: 600 ms per word/nonword (medium-timing) and 750 ms per word/nonword (slow-timing; see **Table 2** for a description of the presentation rates by participant). The presentation speed was determined before the experiment based on the participant's preference. After the last word/nonword in the sequence, a fixation cross was presented for 400 ms, followed by the probe item (1,000 ms for both fast- and slow-timing), and a post-probe fixation (600 ms). Behavioral responses were continually recorded, but only responses 1 second before and 2 seconds after the probe were considered for calculating behavioral performance (**Table 4**). As in Dataset 1, participants performed best on the sentence trials and worse on the nonword-list trials. However, in this sample of participants there was substantial individual variability in the consistency and accuracy of responses (**Table 4**). On average participants provided a correct response 68.57% of the time (**Table 4**). After each trial, a fixation cross was presented for a variable amount of time, semi-randomly selected from a range of durations from 0 to 6,000 ms.

Trials were grouped into runs to give participants short breaks throughout the experiment. In the medium-timing version of the experiment, each run included 36 trials per condition and lasted ~898 s, and in the slow-timing version, each run included 24 trials per condition and lasted 692 s. The total amount of intertrial fixation in each run was 216 s for the medium-timing version and 144 s for the slowest-timing version. One participant (P7) saw a modified slow-timing version of the paradigm where only 48 of the full 72 items per condition were shown. 13 participants completed 2 runs of the experiment (all saw the medium-timing version, 72 trials per condition), 2 participants completed 3 runs of the experiment (one saw the slow-timing version, 72 trials per condition; and the other saw the modified slow-timing version, 48 trials per condition), and 1 participant completed 1 run of the experiment (medium-timing version, 36 trials per condition, **Table 2**).

For all clustering analyses, only the first eight words/nonwords of the stimulus were used to ensure that the length of the timecourses being analyzed was the same across Dataset 1 and 2.

Language-Responsive Electrode Selection

In both datasets, we identified language-responsive electrodes as electrodes that respond significantly more (on average, across trials) to sentences (the S condition) than to perceptually

similar but linguistically uninformative (i.e., meaningless and unstructured) nonword sequences (the N condition). First, the envelope of the high-gamma signal was averaged across word/nonword positions (8 positions in the experiment used in Dataset 1, and 12 positions in the experiment used in Dataset 2) to construct an 'observed' response vector for each electrode (1 x nTrialsS + nTrialsN; the number of trials, across the S and N conditions, varied by participant between 72 and 160). The observed response vector was then correlated (using Spearman's correlation) with an 'idealized' language response vector, where sentence trials were assigned a value of 1 and nonword trials—a value of -1. The values in the ideal response vector were then randomly permuted without replacement and a new correlation was computed. This process was repeated 10,000 times, for each electrode separately, to construct a null distribution (with shuffled labels) relative to which the true correlation between the observed values and the 'idealized' values could be evaluated. Electrodes were determined to be language-responsive if the observed vs. idealized correlation was greater than 95% of the correlations computed using the permuted idealized response vectors (equivalent to $p < 0.05$). (We chose a liberal significance threshold in order to maximize the number of electrodes to be included in the critical analyses, and to increase the chances of discovering distinct response profiles.) The majority of the language-responsive electrodes (98.3% in Dataset 1, 53.9% in Dataset 2) fell in the left hemisphere, but we use electrodes across both hemispheres in all analyses (see e.g., Lipkin et al., 2022 for evidence of a robust right-hemisphere component of the language network in a dataset of >800 participants).

Participants	Age	Sex	Site	ECoG or sEEG	Language-responsive electrodes (S>N)	Total clean electrodes	Total electrodes	Native sampling freq (Hz)	Elec per amp	Runs	Pres. rate (per word)	Trials per cond
Participant 1	29	F	AMc	ECoG	62 (0 RH)	108 (0 RH)	120 (0 RH)	1200	16	10	450ms	80
Participant 2	25	F	AMc	ECoG	17 (0 RH)	115 (0 RH)	128 (0 RH)	1200	16	10	700ms	60
Participant 3	18	F	AMc	ECoG	17 (0 RH)	92 (0 RH)	98 (0 RH)	1200	16	10	700ms	60
Participant 4	28	M	AMc	ECoG	26 (0 RH)	106 (0 RH)	134 (0 RH)	1200	64	10	700ms	60
Participant 5	25	F	AMc	ECoG	48 (0 RH)	93 (0 RH)	98 (0 RH)	1200	64	10	450ms	80
Participant 6	20	F	AMc	ECoG	7 (3 RH)	36 (20 RH)	36 (20 RH)	1200	64	10	450ms	80

Table 1 – Details for Dataset 1. (All data were collected at the Albany Medical Center (Site=AMC).) Here and in Table 2, 'Total electrodes' excludes reference electrodes, ground electrodes, microphone electrodes, trigger electrodes, skull EEG electrodes, and EKG electrodes; and 'Total clean electrodes' excludes electrodes with significant line noise, significant interictal discharges, or large visual artifacts identified through manual inspection. 'Elec per amp' – Number of electrodes per amplifier. 'Pres rate (per word)' – duration of presentation of each single word or nonword.

Participant	Age	Sex	Site	ECoG or sEEG	Language-responsive electrodes (S>N)	Total clean electrodes	Total electrodes	Native sampling freq (Hz)	Elec per amp	Runs	Pres rate (per word)	Trials per cond
Participant 7	51	M	AMc	ECoG	14 (7 RH)	116 (25 RH)	126 (26 RH)	1200	64	3	750ms	48
Participant 8	30	F	AMC	both	18 (0 RH)	76 (1 RH)	92 (3 RH)	1200	64	3	750ms	72
Participant 9	31	M	AMC	sEEG	2 (1 RH)	90 (44 RH)	98 (52 RH)	1200	64	2	600ms	72
Participant 10	59	F	AMC	sEEG	2 (0 RH)	113 (0 RH)	124 (0 RH)	1200	64	2	600ms	72
Participant 11	23	M	AMc	ECoG	58 (33 RH)	209 (110 RH)	216 (110 RH)	1200	64	2	600ms	72
Participant 12	39	M	AMC	sEEG	5 (5 RH)	112 (112 RH)	128 (128 RH)	1200	64	2	600ms	72
Participant 13	29	M	AMc	ECoG	9 (0 RH)	126 (0 RH)	132 (0 RH)	1200	64	2	600ms	72
Participant 14	36	M	AMC	sEEG	3 (2 RH)	169 (84 RH)	184 (90 RH)	1200	64	2	600ms	72
Participant 15	25	M	BJH	sEEG	19 (16 RH)	183 (93 RH)	183 (93 RH)	1000	64	2	600ms	72
Participant 16	38	M	BJH	sEEG	49 (15 RH)	169 (72 RH)	224 (112 RH)	1000	64	2	600ms	72

Participant 17	31	F	BJH	sEEG	17 (0 RH)	228 (30 RH)	228 (30 RH)	1000	64	2	600ms	72
Participant 18	40	M	BJH	sEEG	35 (5 RH)	137 (11 RH)	192 (14 RH)	1000	64	2	600ms	72
Participant 19	66	M	BJH	sEEG	32 (1 RH)	210 (13 RH)	234 (16 RH)	2000	64	2	600ms	72
Participant 20	24	M	BJH	sEEG	7 (0 RH)	156 (30 RH)	218 (30 RH)	2000	64	2	600ms	72
Participant 21	39	M	MCJ	sEEG	11 (1 RH)	108 (45 RH)	109 (45 RH)	1200	64	1	600ms	36
Participant 22	21	F	SLCH	sEEG	81 (81 RH)	176 (176 RH)	186 (186 RH)	2000	64	2	600ms	72

Table 2 – Details for Dataset 2. (The data were collected at four sites: Albany Medical Center (Site=AMC), Barnes-Jewish Hospital (Site=BJH), Mayo Clinic Jacksonville (Site=MCJ), and St. Louis Children's Hospital (Site=SLCH)).

Participant	Trials responded	Sentences	Word-lists	Jabberwocky	Nonword-lists	All conditions
Participant 1	99.69%	97.50%	91.25%	81.01%	78.48%	87.11%
Participant 2	99.17%	100.00%	91.67%	88.33%	72.88%	88.24%
Participant 3	100.00%	100.00%	93.33%	90.00%	78.33%	90.42%
Participant 4	100.00%	100.00%	86.67%	81.67%	71.67%	85.00%
Participant 5	98.75%	45.00%	65.82%	49.37%	52.56%	53.16%
Participant 6	96.25%	93.59%	89.61%	76.62%	68.42%	82.14%
average	**98.98%**	**89.35%**	**86.39%**	**77.83%**	**70.39%**	**81.01%**

Table 3 – Behavioral results for Dataset 1. Percentage of trials where participants in Dataset 1 responded and their accuracy on completed trials.

Participant	Trials responded	Sentences	Nonword-lists	All conditions
Participant 7	79.17%	70.00%	75.00%	72.37%
Participant 8	95.83%	88.41%	81.16%	84.78%
Participant 9	45.83%	50.00%	57.69%	53.03%
Participant 10	98.61%	94.44%	65.71%	80.28%
Participant 11	16.67%	40.00%	44.44%	41.67%
Participant 12	99.31%	93.06%	64.79%	79.02%
Participant 13	86.81%	83.87%	76.19%	80.00%
Participant 14	99.31%	97.18%	79.17%	88.11%
Participant 15	95.14%	71.01%	55.88%	63.50%
Participant 16	0.69%	0.00%	0.00%	0.00%
Participant 17	83.33%	95.16%	79.31%	87.50%
Participant 18	90.97%	92.65%	76.19%	84.73%
Participant 19	100.00%	94.44%	83.33%	88.89%
Participant 20	34.72%	57.14%	36.36%	48.00%
Participant 21	52.78%	46.15%	64.00%	57.89%
Participant 22	98.61%	91.55%	83.10%	87.32%
average	**73.61%**	**72.82%**	**63.90%**	**68.57%**

Table 4 – Behavioral results for Dataset 2. Percentage of trials where participants in Dataset 2 responded and their accuracy on completed trials.

Clustering analysis

Using Dataset 1 (n=6 participants, m=177 language-responsive electrodes), we created a single timecourse per electrode by concatenating the average timecourses across the four conditions (sentences (S), word-lists (W), Jabberwocky sentences (J), nonword-lists (N)). All the timepoints of the concatenated timecourses (864 data points: 60 Hz * 4 conditions * 3.60 seconds per trial after resampling) served as input to a k-medoids clustering algorithm (Kaufman & Rousseuw, 1990). K-medoids is a clustering technique that divides data points—electrodes in our case—into k groups, where k is predetermined. The algorithm attempts to minimize the distances between each electrode and the cluster center, where cluster centers are represented by 'medoids' (exemplar electrodes selected by the algorithm) and the distance metric is correlation-based. K-medoids clustering was chosen over the more commonly used k-means clustering to allow for the use of a correlation-based distance metric as we were most interested in the shape of the timecourses over their scale which can vary due to cognitively irrelevant physiological differences

(but see **Figure S1** for evidence that similar clusters emerge with a k-means clustering algorithm using a Euclidean distance).

Optimal number of clusters

To determine the optimal number of clusters, we used the "elbow" method (e.g., Rokach and Maimon, 2005) which searches for the value of k above which the increase in explained variance becomes more moderate. For each k (between 2 and 10), k-medoids clustering was performed, and explained variance was computed as the sum of the correlation-based distances of all the electrodes to their assigned cluster center and normalized to the sum of the distances for k=1 (equivalent to the variance of the full dataset). This explained variance was plotted against k and the "elbow" was determined as the point after which the derivative became more moderate. We plot the derivative of this curve as well for easier inspection of the transition point. We also repeat the elbow method while enforcing a parametrically sampled reliability threshold (from 0.1 to 0.4 in increments of 0.1) to further examine our choice of k. If the chosen k does, in fact, appropriately describe the data, we would expect the strength of the elbow (that is, the drop in explained variance for k+1) to increase.

Partial correlation of individual electrodes with each of the cluster medoids

To evaluate the extent to which the observed responses can be attributed to a single profile, we computed partial correlations (Fisher, 1924) of every electrode's mean timecourse with that of each of the cluster medoids, while controlling for the other two cluster medoids. For instance, take $r_{s1C1,C2C3}$ as the partial correlation between a signal *s1* and Cluster 1 medoid *C1*, while controlling for the Cluster 2 medoid *C2* and Cluster 3 medoid *C3*. $r_{s1C1,C2C3}$ can be computed by, i) performing a multiple regression analysis with *s1* as the dependent variable and *C2* and *C3* as the independent variables, obtaining the residual *e1*; ii) performing a multiple regression analysis with *C1* as the dependent variable and *C2* and *C3* as the independent variable, obtaining the residual *e2*; and iii.) calculating the correlation coefficient between the residuals *e1* and *e2*. This is the partial correlation $r_{s1C1,C2C3}$. The analysis was performed using the Matlab *partialcorr* function.

Cluster stability across trials

We evaluated the stability of the clustering solution by performing the same clustering procedure as described above (Clustering analysis) on half the trials. To evaluate the similarity of the clusters derived based on only half of the trials to the clusters derived based on all trials, we first had to determine how clusters correspond between any two solutions. In particular, given that the specific order of the clusters that the k-medoids algorithm produces depends on the (stochastic) choice of initial cluster medoids, the electrodes that make up Cluster 1 in one solution may be labeled as Cluster 2 in another solution. To determine cluster correspondence across solutions, we matched the cluster centers (computed here as the average timecourse of all electrodes in a given cluster) from a solution based on half of the trials to the most highly correlated cluster centers from the solution based on all trials.

We then conducted a permutation analysis to statistically compare the clustering solutions. This was done separately for each of the two halves of the data (odd- and even-numbered subsets of

trials). Under the null hypothesis, no distinct response profiles should be detectable in the data, and consequently, responses in one electrode should be interchangeable with responses in another electrode. Using half of the data, we shuffled average responses across electrodes (within each condition separately, thus disrupting the relationship between the conditions for a given electrode while leaving the distribution of within-condition average responses intact), re-clustered the electrodes into 3 clusters, and then correlated the resulting cluster centers to the 'corresponding' cluster centers from the full dataset. This permutation test was determined to be more conservative than shuffling individual trials across electrodes (within each condition separately). However, comparisons remained significant when shuffling individual trials. We repeated this process 1,000 times to construct a null distribution of the correlations for each of the 3 clusters. These distributions were used to calculate the probability that the correlation between the clusters across the two solutions using the actual, non-permuted data was higher than would be expected by chance.

Cluster robustness to data loss

We evaluated the robustness of the clustering solution to loss of electrodes to ensure that the solution was not driven by particular electrodes or participants.

To evaluate the similarity of the clusters derived based on only a subset of language-responsive electrodes to the clusters derived based on all electrodes, we progressively removed electrodes from the full set (n=177) until only 3 electrodes remained (the minimal number of electrodes required to split the data into 3 clusters) in increments of 5. Each subset of electrodes was clustered into 3 clusters, and the cluster centers were correlated with the corresponding cluster centers (see section Cluster stability across trials above) from the full set of electrodes. For each subset of electrodes, we repeated this process 100 times, omitting a different random set of n electrodes with replacement, and computed the average correlation across repetitions.

To statistically evaluate whether the clustering solutions with only a subset of electrodes were more similar to the solution on the full set of electrodes on average (across the 100 repetitions at each subset size) than would be expected by chance, we conducted a permutation analysis like the one described in Cluster stability across trials. In particular, using the full dataset, we shuffled average responses across electrodes (within each condition separately), re-clustered the electrodes into 3 clusters, and then correlated the resulting cluster averages to cluster averages from the actual, non-shuffled data. We repeated this process 1,000 times to construct a null distribution of the correlations for each of the 3 clusters. These distributions were used to calculate the probability that the correlation between the clusters across the two solutions using the actual, non-permuted data (a solution on all the electrodes and a solution on a subset of the electrodes) was higher than would be expected by chance. To err on the conservative side, we chose the null distribution for the cluster with the highest average correlation in the permuted version of the data. For each subset of electrodes, if the average correlation (across the 100 repetitions) fell below the 95th percentile of the null distribution, this was taken to suggest that the clustering solution based on a subset of the electrodes was no longer more correlated to the solution on the full set of electrodes than would be expected by chance.

Electrode locking to onsets of individual word/nonwords

To estimate the degree of stimulus locking for each electrode and condition separately, we fitted a sinusoidal function that represented the stimulus train to the mean of the odd trials and then computed the Pearson correlation between the fitted sinusoidal function and the mean of the even trials. For the sinusoidal function fitting, we assumed that the frequency of the sinusoidal function was the frequency of stimulus presentation and we fitted the phase, amplitude and offset of the sinusoid by searching parameter combinations that minimized the sum of squared differences between the estimated sinusoidal function and the data. Cross-validation (fitting on odd trials and computing the correlation on even trials) ensured non-circularity. To statistically quantify differences in the degree of stimulus locking between the clusters and among the conditions, we ran a linear mixed-effects (LME, using the Matlab procedure *fitlme*) model regressing the locking values of all electrodes and conditions on the fixed effects categorical variable of *cluster* (with 3 levels for Cluster 1, 2 or 3 according to which cluster each electrode was assigned to) and *condition* (with 4 levels for conditions S, W, J, N), both grouped by the random effects variable of *participant*, as well as a fixed interaction term between *cluster* and *condition*:

*Locking ~ 1 + cluster*condition + (cluster|participant) + (condition|participant)*

An ANOVA test for LME was used to determine the main effects of *cluster* and *condition* and their interaction. Pairwise comparisons of all 3 clusters and 4 conditions as well as interactions between all (cluster, condition) pairs were extracted from the model estimates.

Electrode discrimination between conditions

To examine the *timecourse of condition divergence*, as quantified by the electrodes' ability to linearly discriminate between the magnitudes of pairs of conditions. We focused on condition pairs that critically differ in their engagement of particular linguistic processes: conditions S and W, which differ in whether they engage combinatorial (syntactic and semantic) processing (S=yes, W=no), conditions W and N, which differ in whether they engage word meaning processing (W=yes, N=no), and conditions J and N, which differ in whether they engage syntactic processing (J=yes, N=no). This analysis tests how early the relevant pair of conditions reliably diverge and the strength of that divergence. For every electrode, the mean response to the three conditions of interest (S, W, and N) was averaged across 100 ms bins with a ~~50~~ 100 ms sliding window. For each cluster separately, a binary logistic classifier (selected from the best of 20 random instantiations; performed using the Matlab *fitclinear* function) was trained (to discriminate S from W, W from N, or J from N) at each time bin using the binned neural signal up to, and including, that time bin. Each classifier was trained using 10-fold cross validation (train on 90% of the data and test using the remaining 10%, repeated for 10 splits of the data such that every observation was included in the test set exactly once). The predicted and actual conditions across all folds were used to calculate accuracy (the percent of mean responses from all electrodes in a particular cluster correctly classified as S/W, W/N, or J/N). The performance of the model at a given time bin was statistically evaluated using a cluster permutation test to control for multiple comparisons and account for the autocorrelation structure of the signals (Stelzer et al., 2013; Maris & Oostenveld, 2007). This was done by shuffling the condition labels

1000 times for each time bin to simulate surrogate data. For each surrogate data repetition, we computed the sum of consecutive t-values that passed some arbitrary t-value threshold, referred to as the t-sum statistics. We chose a t-value threshold corresponding to an alpha level of 0.05. Using the t-sum values from the 1000 permutations, we constructed a null distribution for this t-sum statistic, and then compared it to the same t-sum statistic computed from the real data to assess significance.

Computing Ngram frequencies of sentence and nonword stimuli

N-gram frequencies were extracted from the Google n-gram online platform (https://books.google.com/ngrams/), averaging across Google books corpora between the years 2010 and 2020. For each individual word, n-gram frequency for n=1 is the frequency of that individual word in the corpus, for n=2 is the frequency of the bigram (sequence of 2 words) ending in, and including, that word, for n=3 is the frequency of the trigram (sequence of 3 words) ending in, and including, that word, etc. Sequences that were not found in the corpus were assigned a value of 0.

Estimation of temporal receptive window size per electrode

We used a simplified model to simulate neural responses in the sentence (S) condition as a convolution of a stimulus train and truncated gaussian kernels with varying widths. The kernels represented an evoked 'response function' with a width (σ) corresponding to the temporal receptive window (TRW) of an idealized neural population underlying the intracranial responses measured by a single electrode. The kernels were constructed from gaussian curves with a standard deviation of $\sigma/2$ truncated at +/- 1 standard deviation (capturing 2/3 of the area under the gaussian). We then normalized the truncated gaussians to have a minimum of 0 and maximum of 1. We chose a symmetric kernel because we wanted to capture the full assumed TRW for a straightforward interpretation of the fitted window size. For instance, a long-tailed response functions would have a shorter "effective" receptive window because the tails of the kernel would affect the neural response much less than the center of the kernel. We further chose a kernel with smooth edges because we assumed that neural activity in response to a stimulus would increase and decrease gradually (cf. an abrupt change of voltage such as in a boxcar shape), given that macroelectrodes sum activity from a large neural population. Furthermore, note that we assumed a fixed TRW, but see Discussion.

We also verified that the specific shape of kernel did not affect our main result. We tested five different response functions: cosine, "wide" Gaussian (Gaussian curves with a standard deviation of $\sigma/2$ that were truncated at +/- 1 standard deviation, as used in the manuscript), "narrow" Gaussian (Gaussian curves with a standard deviation of $\sigma/16$ that were truncated at +/- 8 standard deviations), a square (i.e., boxcar) function (1 for the entire window) and a linear asymmetric function (linear function with a value of 0 initially and a value of 1 at the end of the window).

The stimulus train took a value of 1 at the time of word onsets and 0 otherwise, assuming, for simplicity, that the minimal stimulus unit of interest for language-responsive neural populations is a word (cf. e.g., Bozic et al., 2010 and Regev et al., 2021 for evidence that the language network

is sensitive to sub-lexical structure). Neural responses were simulated for σ ranging from one third of a word to 8 words (the length of our stimuli), in 1 sample increments (1/27th of a word, the highest resolution we were able to evaluate given our sampling rate of 60 Hz). Our implementation of the convolution is identical to assuming that the kernels appear as evoked responses starting at each word onset (https://osf.io/xfbr8/). The length of the evoked response/kernel is directly mapped onto a longer temporal receptive window, such that when a stimulus evokes a wider response its effect will remain for a longer period of time.

To find the best fit of the receptive window size for each electrode after simulating neural signals using this toy model, we selected the TRW size that yielded the highest correlation between the simulated neural response (also normalized to be between 0 and 1) and the actual neural response. The value of the correlation was taken as a proxy for the goodness of fit.

To evaluate significance, we ran linear mixed-effects (LME) models regressing the estimates temporal receptive window sizes (σ) of all electrodes on the fixed effects categorical variable of *cluster* grouped by the random effects variable of *participant*. Cluster was dummy-coded as a categorical variable with three levels, and Cluster 1 was treated as the baseline intercept. This approach allowed us to compare electrodes in Cluster 2 to those in Cluster 1, and electrodes in Cluster 3 to those in Cluster 1. To additionally compare electrodes in Clusters 2 vs. 3, we compared their LME coefficients using the Matlab procedure *coefTest*.

Anatomical topography analysis

We examined the anatomical topographic distribution of the electrodes that exhibit the three temporal response profiles discovered in Dataset 1. Specifically, we probed the spatial relationships between all electrodes that belong to different clusters (e.g., electrodes in Cluster 1 vs. 2) with respect to the two axes: anterior-posterior [y], and inferior-superior [z]. This approach allowed us to ask whether, for example, electrodes that belong to one cluster tend to consistently fall posterior to the electrodes that belong to another cluster.

To do this, we extracted the MNI coordinates of all the electrodes in each of the three clusters and ran linear mixed-effects (LME) models regressing each of the coordinates (either y or z) on the fixed effects categorical variable of *cluster* grouped by the random effects variable of *participant*, using the Wilkinson formula:

Coordinate ~ 1 + cluster + (1 + cluster|participant)

while *Coordinate* is either the y or z MNI coordinate. The random effect that groups the estimates by participant ensures that electrode coordinates are compared *within participants*. This approach is crucial f34or accommodating inter-individual variability in the precise locations of language areas (e.g., Fedorenko et al., 2010), which means that the absolute values of MNI coordinates cannot be easily compared between participants.

Cluster was dummy-coded as a categorical variable with three levels, and Cluster 1 was treated as the baseline intercept. This approach allowed us to compare electrodes in Cluster 2 to those

in Cluster 1, and electrodes in Cluster 3 to those in Cluster 1. To additionally compare electrodes in Clusters 2 vs. 3, we ran another similar LME model with the only difference being that the baseline intercept was now the Cluster 2 category (**Tables S2-4**). To account for the small number of participants in Dataset 1, we used the Satterthwaite corrective degree-of-freedom approximation method, combined with REML fitting for LME, which was shown to be most effective when using the Satterthwaite method (Luke, 2017).

We repeated this analysis for Dataset 2, but we only examined Clusters 1 and 3, which were robustly present in that dataset. We performed the analysis for the electrodes in the two hemispheres separately.

Replication of the clusters in Dataset 2.

As described in Experiment, the design that was used for participants in Dataset 1 included four conditions: sentences (S), word-lists (W), Jabberwocky sentences (J), and nonword-lists (N). Because the design in Dataset 2 included only two of the four conditions (sentences (S) and nonword-lists (N)), we first repeated the clustering procedure for Dataset 1 using only the S and N conditions to test whether similar clusters could be recovered with only a subset of conditions.

We then applied the same clustering procedure to Dataset 2 (n=16 participants, m=362 language-responsive electrodes). The elbow method revealed that the optimal number of clusters in Dataset 2 is k=2. However, because the optimal number of clusters in Dataset 1 was k=3, we examined the clustering solutions at both k=2 and k=3 levels. We also performed an analysis where we assigned electrodes in Dataset 2 to the most correlated Dataset 1 cluster. This analysis was intended to examine whether responses like those found in Dataset 1 were at all present in Dataset 2 (even if they did not emerge as strongly through clustering), and thus the assignment of electrodes to a 'cluster' was done by correlation alone – no actual clustering was performed.

To statistically compare the clustering solutions between Datasets 1 and 2 for k=3 and following the assignment by correlation procedure, we used the same approach as the one described above (Stability of clusters across trials). In particular, using Dataset 2, we shuffled average responses across electrodes (within each condition separately), re-clustered or re-assigned the electrodes into 3 clusters, and then correlated the resulting cluster averages to the cluster averages from Dataset 1. We repeated this process 1,000 times to construct a null distribution of the correlations for each of the 3 clusters. These distributions were used to calculate the probability that the correlation between the clusters across the two datasets using the actual, non-permuted Dataset 2 was higher than would be expected by chance.

To statistically compare the clustering solutions when k=3 in Dataset 1 and k=2 in Dataset 2, we used a similar procedure as the one described above. However, we only compared the resulting cluster centers from the permuted data to the two clusters in Dataset 1 that were most strongly correlated with the two clusters that emerged from Dataset 2 (i.e., Clusters 1 and 3).

Data Availability

Preprocessed data will be publicly available on OpenNeuro at the time of publication. All stimuli and statistical results are available on OSF at https://osf.io/xfbr8/. Raw data will be made available upon request.

Code Availability

Code used to conduct analyses and generate figures from the preprocessed data will be publicly available on GitHub at the time of publication.

Acknowledgements

We would like to acknowledge the participants for agreeing to take part in our study, as well as Nancy Kanwisher, former and current EvLab members, especially Cory Shain and Anya Ivanova, and the audience at the Neurobiology of Language conference (2022, Philadelphia) for helpful discussions and comments on the analyses and manuscript. TIR was supported by the Zuckerman-CHE STEM Leadership Program and by the Poitras Center for Psychiatric Disorders Research. CC was supported by the Kempner Institute for the Study of Natural and Artificial Intelligence at Harvard University. ALR was supported by NIH award U01-NS108916. JTW was supported by NIH awards R01-MH120194 and P41-EB018783, and the American Epilepsy Society Research & Training Fellowship for clinicians. PB was supported by NIH awards R01-EB026439, U24-NS109103, U01-NS108916, U01-NS128612 and P41-EB018783, the McDonnell Center for Systems Neuroscience and Fondazione Neurone. EF was supported by NIH awards R01-DC016607, R01-DC016950, and U01-NS121471 and research funds from the McGovern Institute for Brain Research, Brain and Cognitive Sciences Department, and the Simons Center for the Social Brain.

Author Contribution Statement

TIR and CC equally contributed to study conception and design, data analysis and interpretation of results, and manuscript writing; EH contributed to data analysis and manuscript editing; MA to data collection and analysis; ALR, JW and PB to data collection and manuscript editing; EF contributed to study conception and design, supervision, interpretation of results, and manuscript writing.

Competing Interests Statement

The authors declare no competing interests.

References

Adamek M, Swift JR, Brunner P (2022). VERA - Versatile Electrode Localization Framework.

Anderson, A. J., Kiela, D., Binder, J. R., Fernandino, L., Humphries, C. J., Conant, L. L., Raizada, R. D., Grimm, S., & Lalor, E. C. (2021). Deep Artificial Neural Networks Reveal a Distributed Cortical Network Encoding Propositional Sentence-Level Meaning. *J Neurosci*, *41*(18), 4100-4119.

Arnon I, Snider N (2010). More than words: Frequency effects for multi-word phrases. J Mem Lang 62:67–82.

Avants BB, Epstein CL, Grossman M, Gee JC (2008). Symmetric diffeomorphic image registration with cross-correlation: evaluating automated labeling of elderly and neurodegenerative brain. Medical image analysis. 12(1):26-41.

Baker CI, Liu J, Wald LL, Kwong KK, Benner T, Kanwisher N (2007). Visual word processing and experiential origins of functional selectivity in human extrastriate cortex. Proc Natl Acad Sci USA 104:9087–9092.

Baldassano C, Chen J, Zadbood A, Pillow JW, Hasson U, Norman KA (2017). Discovering Event Structure in Continuous Narrative Perception and Memory. Neuron 95(3):709–721.

Baldassano C, Hasson U, Norman KA (2018). Representation of Real-World Event Schemas during Narrative Perception. J Neurosci 38(45):9689–9699.

Bautista A, Wilson SM (2016). Neural responses to grammatically and lexically degraded speech. Lang Cogn Neurosci 31:567–574.

Bedny M, Pascual-Leone A, Dodell-Feder D, Fedorenko E, Saxe R (2011). Language processing in the occipital cortex of congenitally blind adults. Proc Natl Acad Sci USA 108:4429–4434.

Blank I, Balewski Z, Mahowald K, Fedorenko E (2016) Syntactic processing is distributed across the language system. Neuroimage 127:307–323.

Blank I, Kanwisher N, Fedorenko E (2014). A functional dissociation between language and multiple-demand systems revealed in patterns of BOLD signal fluctuations. J Neurophysiol 112:1105–1118.

Blank IA, Fedorenko E (2020). No evidence for differences among language regions in their temporal receptive windows. Neuroimage 219.

Bozic, M., Tyler, L. K., Ives, D. T., Randall, B., & Marslen-Wilson, W. D. (2010). Bihemispheric foundations for human speech comprehension. Proc Natl Acad Sci USA 107(40):17439–17444.

Braga RM, DiNicola LM, Becker HC, Buckner RL (2020). Situating the left-lateralized language network in the broader organization of multiple specialized large-scale distributed networks. J Neurophysiol 124:1415–1448.

Buckner RL, DiNicola LM (2019). The brain's default network: updated anatomy, physiology and evolving insights. Nat Rev Neurosci 20(10):593–608.

Bybee J (1999). Usage-based Phonology. In: Functionalism and Formalism in Linguistics: Volume I: General papers, pp 211–242. John Benjamins Publishing.

Bybee J (2013). Usage-based theory and exemplar representations of constructions. In: The Oxford Handbook of Construction Grammar, pp 49–69.

Caucheteux, C., Gramfort, A., & King, J. R. (2021). Disentangling Syntax and Semantics in the Brain with Deep Networks. *arXiv*.

Caucheteux, C., Gramfort, A. & King, JR (2023). Evidence of a predictive coding hierarchy in the human brain listening to speech. Nat Hum Beh 7(3):430-441

Chaudhuri, R., Knoblauch, K., Gariel, M. A., Kennedy, H., & Wang, X. J. (2015). A Large-Scale Circuit Mechanism for Hierarchical Dynamical Processing in the Primate Cortex. Neuron 88(2): 419–431.

Chang, C. H. C., Nastase, S. A., & Hasson, U. (2022). Information flow across the cortical timescale hierarchy during narrative construction. Proc Natl Acad Sci USA 119(51):e2209307119.

Chen X, Affourtit J, Ryskin R, Regev TI, Norman-Haignere S, Jouravlev O, Malik-Moraleda S, Kean H, Varley R, Fedorenko E (2021). The human language system does not support music processing. bioRxiv:2021.06.01.446439.

Cheung C, Ivanova A, Siegelman M, Pongos A, Kean H, Fedorenko E (2020). The effect of task on sentence processing in the brain. In: Poster Presentation at the Society for the Neurobiology of Language.

Chien, H. S., & Honey, C. J. (2020). Constructing and Forgetting Temporal Context in the Human Cerebral Cortex. Neuron 106(4):675–686.

Dapretto M, Bookheimer SY (1999). Form and Content: Dissociating Syntax and Semantics in Sentence Comprehension. Neuron 24:427–432.

Deen B, Koldewyn K, Kanwisher N, Saxe R (2015). Functional organization of social perception and cognition in the superior temporal sulcus. Cereb Cortex 25:4596–4609.

Desbordes, T., Lakretz, Y., Chanoine, V., Oquab, M., Badier, J. M., Trébuchon, A., Carron, R., Bénar, C. G., Dehaene, S., & King, J. R. (2023). Dimensionality and Ramping: Signatures of Sentence Integration in the Dynamics of Brains and Deep Language Models. *J Neurosci 43*(29):5350–5364.

DeWitt I, Rauschecker JP (2012). Phoneme and word recognition in the auditory ventral stream. Proc Natl Acad Sci USA 109:2709.

Diachek E, Blank I, Siegelman M, Affourtit J, Fedorenko E (2020). The domain-general multiple demand (MD) network does not support core aspects of language comprehension: A large-scale fMRI investigation. J Neurosci 40:4536–4550.

Dichter BK, Breshears JD, Leonard MK, Chang EF (2018). The Control of Vocal Pitch in Human Laryngeal Motor Cortex. Cell 174:21-31.

Dick F, Bates E, Utman JA, Wulfeck B, Dronkers N, Gernsbacher MA (2001). Language deficits, localization, and grammar: Evidence for a distributive model of language breakdown in aphasic patients and neurologically intact individuals. Psychol Rev 108:759–788.

Embick D, Marantz A, Miyashita Y, O'Neil W, Sakai KL (2000). A syntactic specialization for Broca's area. Proc Natl Acad Sci USA 97:6150–6154.

Evans N, Levinson SC (2009). The myth of language universals: Language diversity and its importance for cognitive science. Behavioral and brain sciences. 32(5):429-48.

Fedorenko E, Behr MK, Kanwisher N (2011). Functional specificity for high-level linguistic processing in the human brain. Proc Natl Acad Sci USA 108:16428–16433.

Fedorenko E, Blank IA. Broca's area is not a natural kind (2020). Trends in cognitive sciences. 24(4):270-84.

Fedorenko E, Blank IA, Siegelman M, Mineroff Z (2020). Lack of selectivity for syntax relative to word meanings throughout the language network. Cognition 203:104348.

Fedorenko E, Hsieh PJ, Nieto-Castañón A, Whitfield-Gabrieli S, Kanwisher N (2010). New method for fMRI investigations of language: Defining ROIs functionally in individual subjects. J Neurophysiol 104:1177–1194.

Fedorenko E, Nieto-Castañon A, Kanwisher N (2012). Lexical and syntactic representations in the brain: An fMRI investigation with multi-voxel pattern analyses. Neuropsychologia 50:499–513.

Fedorenko E, Scott TL, Brunner P, Coon WG, Pritchett B, Schalk G, Kanwisher N (2016). Neural correlate of the construction of sentence meaning. Proc Natl Acad Sci USA 113:E6256–E6262.

Friederici AD (2002). Towards a neural basis of auditory sentence processing. Trends Cogn Sci 6:78–84.

Friederici AD (2011). The brain basis of language processing: From structure to function. Physiol Rev 91:1357–1392.

Friederici AD, Meyer M, Von Cramon DY (2000). Auditory Language Comprehension: An Event-Related fMRI Study on the Processing of Syntactic and Lexical Information. Brain Lang 74:289–300.

Gibson E, Bergen L, Piantadosi ST (2013). Rational integration of noisy evidence and prior semantic expectations in sentence interpretation. Proc Natl Acad Sci USA 110(20):8051-8056.

Gibson E, Tan C, Futrell R, Mahowald K, Konieczny L, Hemforth B, Fedorenko E (2017). Don't Underestimate the Benefits of Being Misunderstood. Psychol Sci 28(6):703–712.

Gibson E, Futrell R, Piantadosi SP, Dautriche I, Mahowald K, Bergen L, Levy R (2019). How Efficiency Shapes Human Language. Trends Cogn Sci 23(5):389–407.

Giglio L, Ostarek M, Weber K, Hagoort P (2022). Commonalities and asymmetries in the neurobiological infrastructure for language production and comprehension. Cerebral Cortex. 32(7):1405-18.

Goldberg AE (2003). Constructions: A new theoretical approach to language. Trends Cogn Sci 7:219–224.

Goldstein A et al. (2022). Shared computational principles for language processing in humans and deep language models. Nat Neurosci 25:369–380.

Goldstein A et al. (2023). Deep speech-to-text models capture the neural basis of spontaneous speech in everyday conversations. bioRxiv: 2023.06.26.546557.

Graves WW, Grabowski TJ, Mehta S, Gupta P (2008). The left posterior superior temporal gyrus participates specifically in accessing lexical phonology. J Cogn Neurosci 20:1698–1710.

Grodzinsky Y, Santi A (2008). The battle for Broca's region. Trends Cogn Sci 12:474–480.

Hagoort P (2005) On Broca, brain, and binding: a new framework. Trends Cogn Sci 9:416–423.

Hamamé CM, Szwed M, Sharman M, Vidal JR, Perrone-Bertolotti M, Kahane P, Bertrand O, Lachaux JP (2013). Dejerine's reading area revisited with intracranial EEG. Neurology 80:602–603.

Hasson U, Yang E, Vallines I, Heeger DJ, Rubin N (2008). A Hierarchy of Temporal Receptive Windows in Human Cortex. J Neurosci 28:2539–2550.

Hu J, Small H, Kean H, Takahashi A, Zekelman L, Kleinman D, Ryan E, Nieto-Castañón A, Ferreira V, Fedorenko E (2023). Precision fMRI reveals that the language-selective network supports

both phrase-structure building and lexical access during language production. Cerebral Cortex. 33(8):4384-404.

Humphries C, Willard K, Buchsbaum B, Hickok G (2001). Role of anterior temporal cortex in auditory sentence comprehension: an fMRI study. Neuroreport 12:1749–1752.

Huth AG, De Heer WA, Griffiths TL, Theunissen FE, Gallant JL (2016). Natural speech reveals the semantic maps that tile human cerebral cortex. Nature 532:453–458.

Ivanova AA (2022). The role of language in broader human cognition: evidence from neuroscience. Ch. 5. Doctoral dissertation, Massachusetts Institute of Technology.

Ivanova AA, Mineroff Z, Zimmerer V, Kanwisher N, Varley R, Fedorenko E (2021). The Language Network Is Recruited but Not Required for Nonverbal Event Semantics. Neurobiol Lang 2:176–201.

Ivanova AA, Srikant S, Sueoka Y, Kean HH, Dhamala R, O'Reilly UM, Bers MU, Fedorenko E (2020). Comprehension of computer code relies primarily on domain-general executive brain regions. elife 9:1–24.

Jackendoff R (2007). A Parallel Architecture perspective on language processing. Brain Res 1146:2–22.

Jackendoff R, Audring J (2020). Morphology and Memory: Toward an Integrated Theory. Top Cogn Sci 12:170–196.

Jacoby N, Fedorenko E (2018) Discourse-level comprehension engages medial frontal Theory of Mind brain regions even for expository texts. Lang Cogn Neurosci 35:780–796.

Jain S, Vo VA, Mahto S, LeBel A, Turek JS, Huth AG (2020). Interpretable multi-timescale models for predicting fMRI responses to continuous natural speech. Adv Neural Inf Process Syst 2020-Decem:1–12.

Janca R, Jezdik P, Cmejla R, Tomasek M, Worrell GA, Stead M, Wagenaar J, Jefferys JGR, Krsek P, Komarek V, Jiruska P, Marusic P (2015). Detection of interictal epileptiform discharges using signal envelope distribution modelling: application to epileptic and non-epileptic intracranial recordings. Brain Topogr 28:172–183.

Keshishian, M., Akkol, S., Herrero, J., Bickel, S., Mehta, A. D., & Mesgarani, N. (2023). Joint, distributed and hierarchically organized encoding of linguistic features in the human auditory cortex. Nat Hum Beh 7(5): 740–753.

Keshev M, Meltzer-Asscher A (2021). Noisy is better than rare: Comprehenders compromise subject-verb agreement to form more probable linguistic structures. Cogn Psychol 124:101359.

Kučera H, Francis W, Twaddell WF, Marckworth ML, Bell LM, Carroll JB. (1967) Computational analysis of present-day American English.

Kuperberg GR, McGuire PK, Bullmore ET, Brammer MJ, Rabe-Hesketh S, Wright IC, Lythgoe DJ, Williams SCR, David AS (2000). Common and Distinct Neural Substrates for Pragmatic, Semantic, and Syntactic Processing of Spoken Sentences: An fMRI Study. J Cogn Neurosci 12:321–341.

Lee EK, Brown-Schmidt S, Watson DG (2013). Ways of looking ahead: hierarchical planning in language production. Cognition 129(3):544-62.

Leonard MK, Gwilliams L, Sellers KK, Chung JE, Xu D, Mischler G, Mesgarani N, Welkenhuysen M, Dutta B, Chang EF (2023). Large-scale single-neuron speech sound encoding across the depth of human cortex. Nature, 110.

Lerner Y, Honey CJ, Silbert LJ, Hasson U (2011). Topographic Mapping of a Hierarchy of Temporal Receptive Windows Using a Narrated Story. J Neurosci 31:2906–2915.

Levy R (2008a). A Noisy-Channel Model of Human Sentence Comprehension under Uncertain Input. In Proceedings of the 2008 Conference on Empirical Methods in Natural Language Processing, pages 234–243, Honolulu, Hawaii. Association for Computational Linguistics.

Levy R (2008b). Expectation-based syntactic comprehension. Cognition 106(3):1126–1177.

Lipkin B, Tuckute G, Affourtit J, Small H, Mineroff Z, Kean H, Jouravlev O, Rakocevic L, Pritchett B, Siegelman M, Hoeflin C, Pongos A, Blank IA, Struhl MK, Ivanova A, Shannon S, Sathe A, Hoffmann M, Nieto-Castañón A, Fedorenko E (2022). Probabilistic atlas for the language network based on precision fMRI data from >800 individuals. Scientific Data 9(1):529.

Liu X, Vermeylen L, Wisniewski D, Brysbaert M (2020). The contribution of phonological information to visual word recognition: Evidence from Chinese phonetic radicals. Cortex 133:48–64.

Lopopolo A, Frank SL, Van Den Bosch A, Willems RM (2017). Using stochastic language models (SLM) to map lexical, syntactic, and phonological information processing in the brain. PLoS One 12:e0177794.

Luke SG. Evaluating significance in linear mixed-effects models in R (2017). Behavior research methods. 49:1494-502.

Maris E, Oostenveld R (2007). Nonparametric statistical testing of EEG-and MEG-data. Journal of neuroscience methods. 164(1):177-90.

Matchin W, Hickok G (2020). The Cortical Organization of Syntax. Cereb Cortex 30:1481–1498.

Mazoyer BM, Tzourio N, Frak V, Syrota A, Murayama N, Levrier O, Salamon G, Dehaene S, Cohen L, Mehler J (1993). The Cortical Representation of Speech. J Cogn Neurosci 5:467–479.

Menenti L, Gierhan SM, Segaert K, Hagoort P (2011). Shared language: overlap and segregation of the neuronal infrastructure for speaking and listening revealed by functional MRI. Psychological science, *22*(9), 1173-1182.

Mesulam MM, Wieneke C, Hurley R, Rademaker A, Thompson CK, Weintraub S, Rogalski EJ (2013). Words and objects at the tip of the left temporal lobe in primary progressive aphasia. Brain 136:601–618.

Mollica F, Piantadosi ST (2019). Humans store about 1.5 megabytes of information during language acquisition. R Soc Open Sci 6: 181393.

Monti MM, Parsons LM, Osherson DN (2012). Thought Beyond Language: Neural Dissociation of Algebra and Natural Language. Psychol Sci 23:914–922.

Mukamel R, Fried I (2011). Human Intracranial Recordings and Cognitive Neuroscience. Annu Rev Psychol 63:511–537.

Murray JD, Bernacchia A, Freedman DJ, Romo R, Wallis JD, Cai X, Padoa-Schioppa C, Pasternak T, Seo H, Lee D, & Wang XJ (2014). A hierarchy of intrinsic timescales across primate cortex. Nat Neuro 17(12):1661–1663.

Nelson MJ, Karoui I El, Giber K, Yang X, Cohen L, Koopman H, Cash SS, Naccache L, Hale JT, Pallier C, Dehaene S (2017). Neurophysiological dynamics of phrase-structure building during sentence processing. Proc Natl Acad Sci USA 114:E3669–E3678.

Norman-Haignere S, Kanwisher NG, McDermott JH (2015). Distinct Cortical Pathways for Music and Speech Revealed by Hypothesis-Free Voxel Decomposition. Neuron 88(6):1281-1296.

Norman-Haignere SV, Long LK, Devinsky O, Doyle W, Irobunda I, Merricks EM, Feldstein NA, McKhann GM, Schevon CA, Flinker A, Mesgarani N (2022). Multiscale temporal integration organizes hierarchical computation in human auditory cortex. Nat Hum Behav 6(3):455–469.

Okada K, Hickok G (2006). Identification of lexical-phonological networks in the superior temporal sulcus using functional magnetic resonance imaging. Neuroreport 17:1293–1296.

Okada K, Matchin W, Hickok G (2017). Phonological feature repetition suppression in the left inferior frontal gyrus. J Cogn Neurosci 30:1549–1557.

Overath T, McDermott JH, Zarate JM, Poeppel D (2015). The cortical analysis of speech-specific temporal structure revealed by responses to sound quilts. Nat Neurosci 18:903–911.

Ryskin R, Futrell R, Kiran S, Gibson E (2018). Comprehenders model the nature of noise in the environment. Cognition 181:141–150.

Ryskin R, Stearns L, Bergen L, Eddy M, Fedorenko E, Gibson E (2021). An ERP index of real-time error correction within a noisy-channel framework of human communication. Neuropsychologia 158:107855.

Pallier C, Devauchelle AD, Dehaene S (2011). Cortical representation of the constituent structure of sentences. Proc Natl Acad Sci USA 108:2522–2527.

Paulesu E, Frith CD, Frackowiak RSJ (1993). The neural correlates of the verbal component of working memory. Nature 362:342–345.

Paulk AC, Kfir Y, Khanna AR, Mustroph ML, Trautmann EM, Soper DJ, Stavisky SD, Welkenhuysen M, Dutta B, Shenoy K V., Hochberg LR, Richardson RM, Williams ZM, Cash SS (2022). Large-scale neural recordings with single neuron resolution using Neuropixels probes in human cortex. Nat Neurosci 2022 252 25:252–263.

Paunov AM, Blank IA, Fedorenko E (2019). Functionally distinct language and theory of mind networks are synchronized at rest and during language comprehension. J Neurophysiol 121:1244–1265.

Price CJ, Moore CJ, Humphreys GW, Wise RJS (1997). Segregating semantic from phonological processes during reading. J Cogn Neurosci 9:727–733.

Reddy AJ, & Wehbe L (2021). Can fMRI reveal the representation of syntactic structure in the brain? *Advances in Neural Information Processing Systems* (Vol. 34, pp. 9843–9856).

Regev M, Honey CJ, Simony E, Hasson U (2013). Selective and invariant neural responses to spoken and written narratives. J Neurosci 33:15978–15988.

Regev TI, Affourtit J, Chen X, Schipper AE, Bergen L, Mahowald K, Fedorenko E (2021). High-level language brain regions are sensitive to sub-lexical regularities. bioRxiv:2021.06.11.447786.

Rodd JM, Davis MH, Johnsrude IS (2005). The Neural Mechanisms of Speech Comprehension: fMRI studies of Semantic Ambiguity. Cereb Cortex 15:1261–1269.

Rokach L, Maimon O (2005). Clustering methods. In: The data mining and knowledge discovery handbook, pp 321–352. Boston, MA.: Springer.

Runyan, CA, Piasini E, Panzeri S, Harvey CD (2017). Distinct timescales of population coding across cortex. Nature 548(7665):92–96.

Saxe R, Brett M, Kanwisher N (2006). Divide and conquer: A defense of functional localizers. Neuroimage 30:1088–1096.

Segaert K, Menenti L, Weber K, Petersson KM, Hagoort P (2012). Shared syntax in language production and language comprehension—an fMRI study. Cerebral Cortex. 22(7):1662-70.

Schalk G, McFarland DJ, Hinterberger T, Birbaumer N, Wolpaw JR (2004). BCI2000: A general-purpose brain-computer interface (BCI) system. IEEE Trans Biomed Eng 51:1034–1043.

Schrimpf M, Blank IA, Tuckute G, Kauf C, Hosseini EA, Kanwisher N, Tenenbaum JB, Fedorenko E (2021). The neural architecture of language: Integrative modeling converges on predictive processing. Proc Natl Acad Sci USA 118.

Scott TL, Gallée J, Fedorenko E (2017). A new fun and robust version of an fMRI localizer for the frontotemporal language system. Cogn Neurosci 8:167–176.

Shain C, Blank IA, Fedorenko E, Gibson E, Schuler W (2022a). Robust Effects of Working Memory Demand during Naturalistic Language Comprehension in Language-Selective Cortex. J Neurosci 42:7412–7430.

Shain C, Blank IA, van Schijndel M, Schuler W, Fedorenko E (2020). fMRI reveals language-specific predictive coding during naturalistic sentence comprehension. Neuropsychologia 138:107307.

Shain C, Kean H, Casto C, Lipkin B, Affourtit J, Siegelman M, Mollica F, Fedorenko E (2023). Graded sensitivity to structure and meaning throughout the human language network. bioRxiv:2021.11.12.467812.

Shain C, Meister C, Pimentel T, Cotterell R, Levy RP (2022b). Large-scale evidence for logarithmic effects of word predictability on reading time. PsyArXiv

Shain C, Paunov A, Chen X, Lipkin B, Fedorenko E (2022c). No evidence of theory of mind reasoning in the human language network. bioRxiv:2022.07.18.500516.

Silbert LJ, Honey CJ, Simony E, Poeppel D, Hasson U (2014). Coupled neural systems underlie the production and comprehension of naturalistic narrative speech. Proc Natl Acad Sci USA. 111(43):E4687-96.

Stelzer J, Chen Y, Turner R (2013). Statistical inference and multiple testing correction in classification-based multi-voxel pattern analysis (MVPA): random permutations and cluster size control. Neuroimage. 65:69-82.

Toneva M, Wehbe L (2019). Interpreting and improving natural-language processing (in machines) with natural language-processing (in the brain). Adv Neural Inf Process Syst 2019-Decem:14954–14964.

Tuckute G, Sathe A, Srikant S, Taliaferro M, Wang M, Schrimpf M, Kay K, Fedorenko E (2023). Driving and suppressing the human language network using large language models. bioRxiv: 2023.04.16.537080.

Vagharchakian L, Dehaene-Lambertz G, Pallier C, Dehaene S (2012). A temporal bottleneck in the language comprehension network. J Neurosci 32:9089–9102.

Vandenberghe R, Nobre AC, Price CJ (2002). The Response of Left Temporal Cortex to Sentences. J Cogn Neurosci 14:550–560.

Woolnough O, Donos C, Murphy E, Rollo PS, Roccaforte ZJ, Dehaene S, Tandon N (2023). Spatiotemporally distributed frontotemporal networks for sentence reading. Proc Natl Acad Sci USA *120*(17): e2300252120.

Supplementary Information

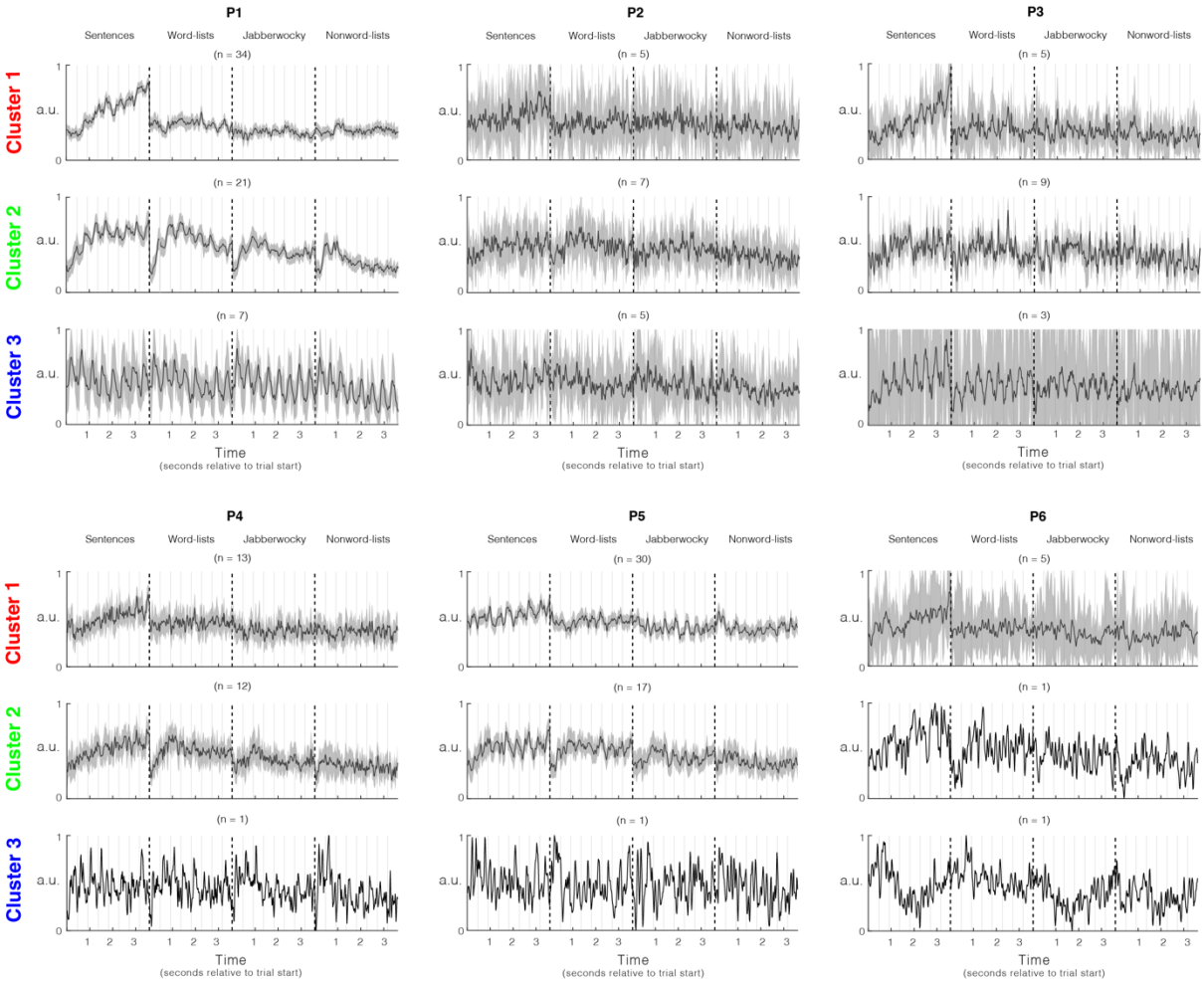

Figure S1 – Dataset 1 k-medoids (k=3) cluster assignments by participant. Average cluster responses as in **Figure 2E** grouped by participant. Shaded areas around the signal reflect a 99% confidence interval over electrodes. The number of electrodes constructing the average (n) is denoted above each signal in parenthesis. Prototypical responses for each of the three clusters are found in nearly all participants individually. However, for participants with only a few electrodes assigned to a given cluster (e.g., P5 Cluster 3), the responses can be more variable.

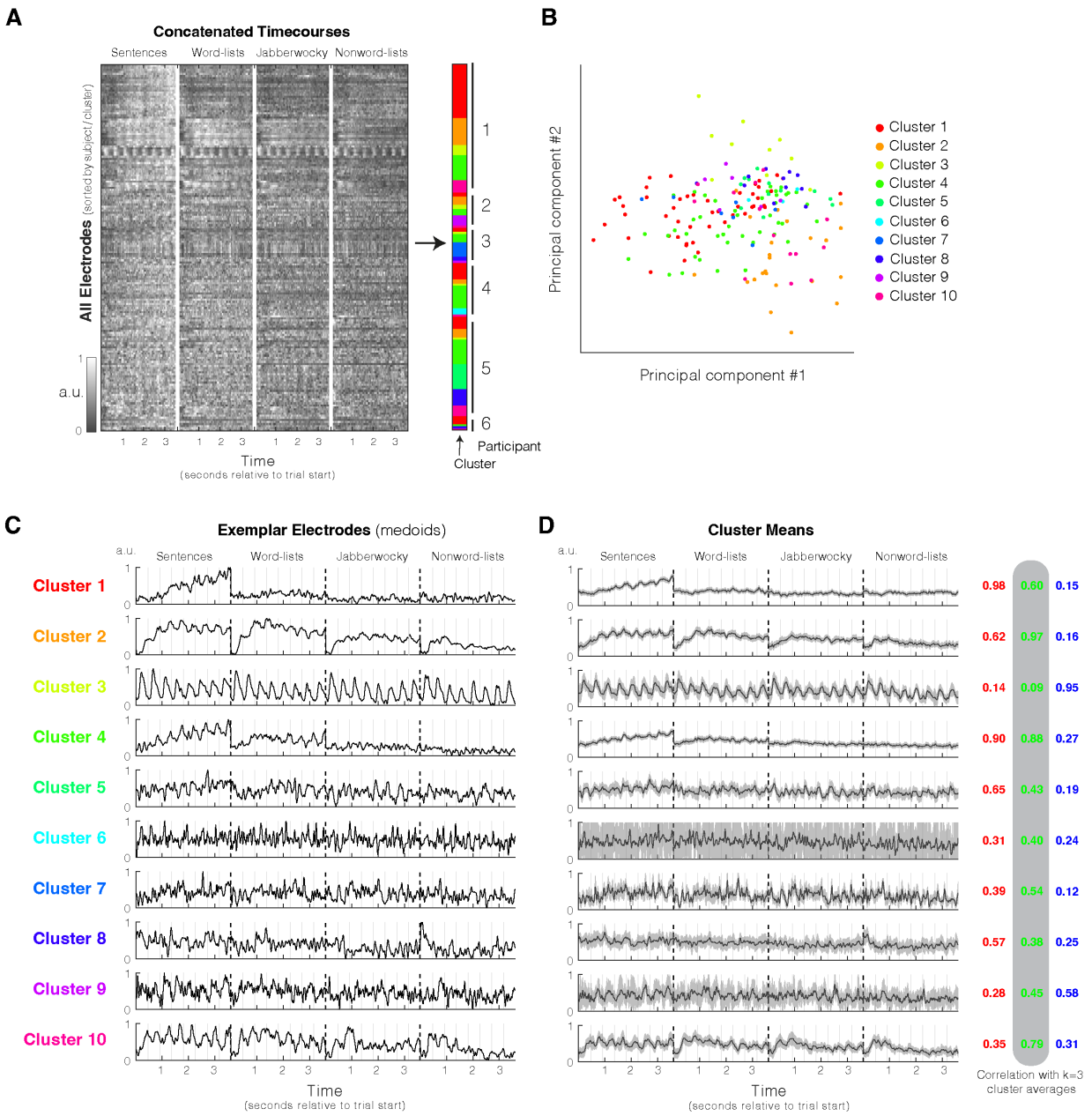

Figure S2 – Dataset 1 k-medoids clustering with k=10. A) Clustering mean electrode responses (S+W+J+N) using k-medoids (k=10) with a correlation-based distance. Shading of the data matrix reflects normalized high-gamma power (70-150Hz). **B)** Electrode responses visualized on their first two principal components, colored by cluster. **C)** Timecourses of best representative electrodes ('medoids') selected by the algorithm from each of the ten clusters. **D)** Timecourses averaged across all electrodes in each cluster. Shaded areas around the signal reflect a 99% confidence interval over electrodes. Many of the additional clusters resemble the main three response profiles from **Figure 2**.

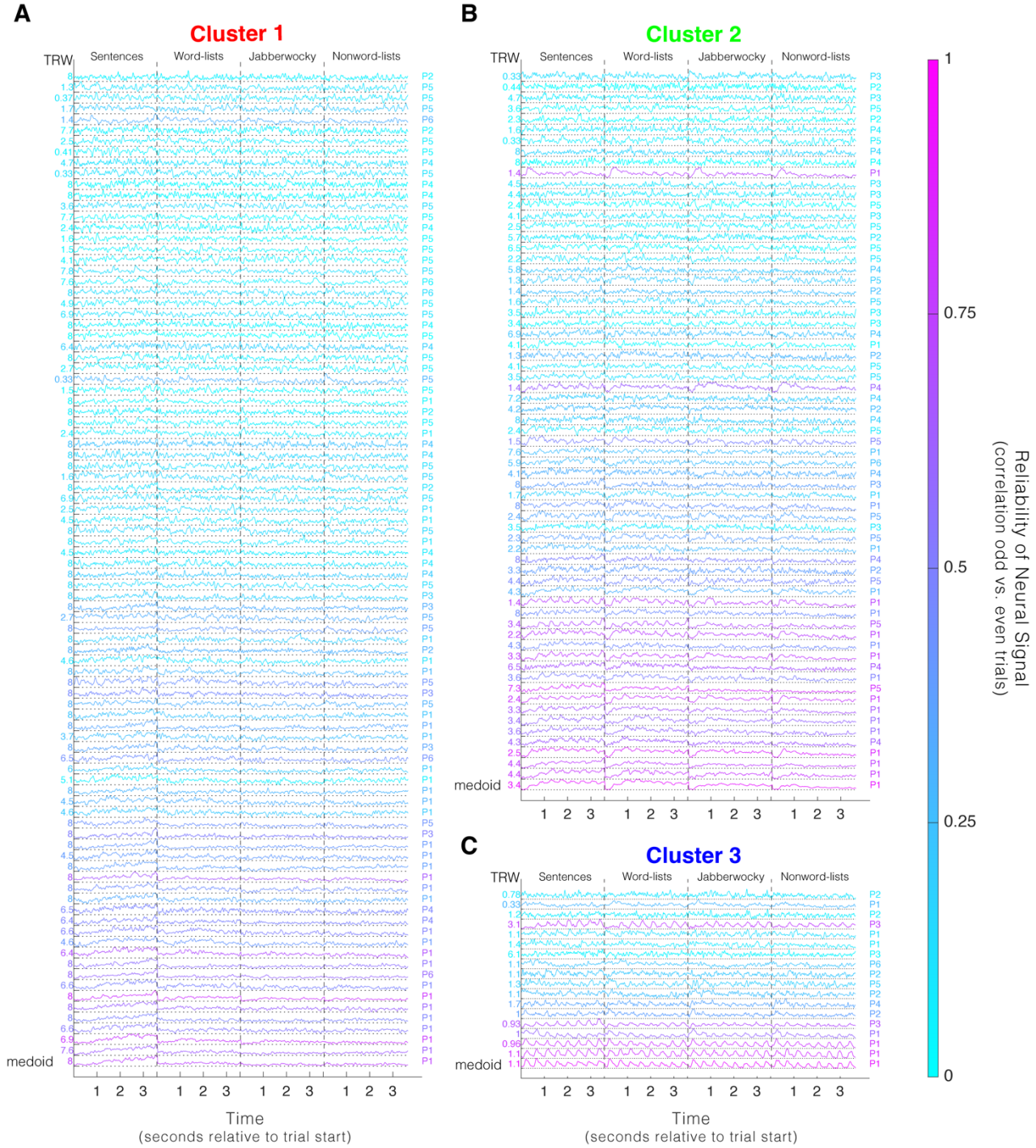

Figure S3 – All Dataset 1 responses. A-C) All Dataset 1 electrode responses. The timecourses (concatenated across the four conditions, ordered: Sentences, Word-lists, Jabberwocky, Nonword-lists) of all electrodes in Dataset 1 sorted by their correlation to the cluster medoid (shown at the bottom of each cluster). Colors reflect the reliability of the measured neural signal, computed by correlating responses to odd and even trials (**Figure 2D**). The estimated temporal receptive window (TRW) using the toy model from **Figure 4** is displayed to the left, and the participant who contributed the electrode is displayed to the right. There is strong consistency in the responses from individual electrodes within a cluster (with more variability in the less reliable electrodes), and electrodes with responses that

are more similar to the cluster medoid tend to be more reliable (more pink). Note that there are two main response profiles that seem reliable (relatively pink) and show a pattern that is distinct from the three prototypical response profiles: One electrode in Cluster 2 that seems to respond only to the onset of the first word/nonword in each trial; and one electrode in Cluster 3 that seems to be highly locked to the onsets off all *but* the first word/nonword. These electrodes highlight that the clusters that we uncovered may not be the *only* responses that exist within the language network, however, the rarity of these responses also emphasizes that the clusters that we uncovered do seem to capture a substantial amount of functional heterogeneity of response patterns in the language network.

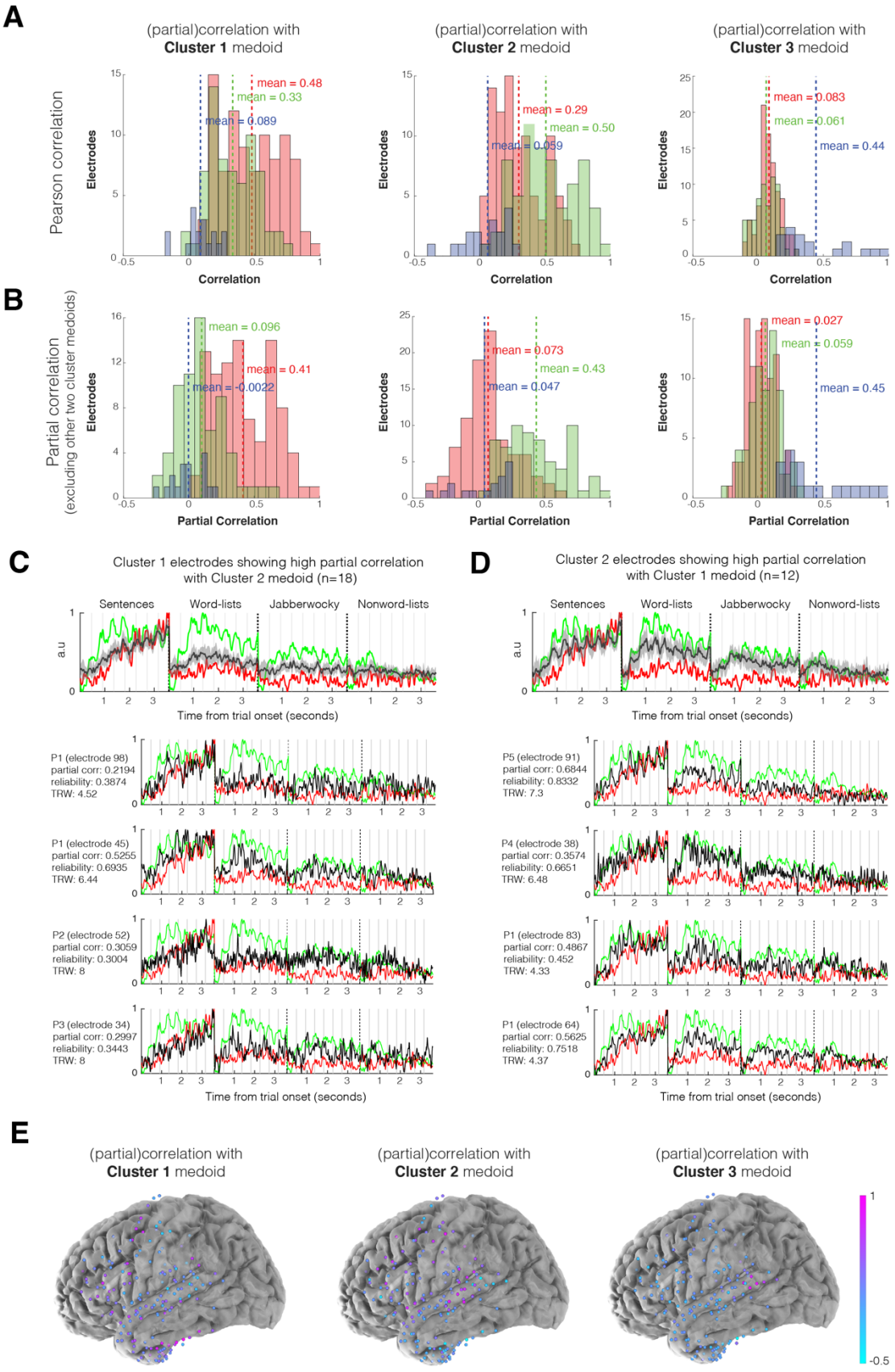
A
(partial)correlation with Cluster 1 medoid
(partial)correlation with Cluster 2 medoid
(partial)correlation with Cluster 3 medoid
Pearson correlation
Electrodes
Correlation
mean = 0.48
mean = 0.33
mean = 0.089
mean = 0.29
mean = 0.50
mean = 0.059
mean = 0.083
mean = 0.061
mean = 0.44
B
Partial correlation
(excluding other two cluster medoids)
Partial Correlation
mean = 0.096
mean = 0.41
mean = -0.0022
mean = 0.073
mean = 0.43
mean = 0.047
mean = 0.027
mean = 0.059
mean = 0.45
C
Cluster 1 electrodes showing high partial correlation with Cluster 2 medoid (n=18)
Sentences
Word-lists
Jabberwocky
Nonword-lists
a.u
Time from trial onset (seconds)
P1 (electrode 98)
partial corr: 0.2194
reliability: 0.3874
TRW: 4.52
P1 (electrode 45)
partial corr: 0.5255
reliability: 0.6935
TRW: 6.44
P2 (electrode 52)
partial corr: 0.3059
reliability: 0.3004
TRW: 8
P3 (electrode 34)
partial corr: 0.2997
reliability: 0.3443
TRW: 8
D
Cluster 2 electrodes showing high partial correlation with Cluster 1 medoid (n=12)
P5 (electrode 91)
partial corr: 0.6844
reliability: 0.8332
TRW: 7.3
P4 (electrode 38)
partial corr: 0.3574
reliability: 0.6651
TRW: 6.48
P1 (electrode 83)
partial corr: 0.4867
reliability: 0.452
TRW: 4.33
P1 (electrode 64)
partial corr: 0.5625
reliability: 0.7518
TRW: 4.37
E
(partial)correlation with Cluster 1 medoid
(partial)correlation with Cluster 2 medoid
(partial)correlation with Cluster 3 medoid
1
-0.5

Figure S4 – Partial correlations of individual response profiles with each of the cluster medoids. **A)** Standard Pearson correlations of all response profiles with each of the cluster medoids, grouped by cluster assignment. **B)** Partial correlations (Methods) of all response profiles with each of the cluster medoids, controlling for the other two cluster medoids, grouped by cluster assignment. **C)** Response profiles from electrodes assigned to Cluster 1 that have a high partial correlation (>0.2, arbitrarily defined) with the Cluster 2 medoid (and split-half reliability>0.3). *Top:* Average over all electrodes that meet these criteria (n=18, black). The Cluster 1 medoid is shown in red, and the Cluster 2 medoid is shown in green. *Bottom:* Four sample electrodes (black). **D)** Response profiles assigned to Cluster 2 that have a high partial correlation (>0.2, arbitrarily defined) with the Cluster 1 medoid (and split-half reliability>0.3). *Top*: Average over all electrodes that meet these criteria (n=12, black). The Cluster 1 medoid is shown in red, and the Cluster 2 medoid is shown in green. *Bottom:* Four sample electrodes (black; see osf.io/xfbr8/ for all mixed response profiles with split-half reliability>0.3). **E)** Anatomical distribution of electrodes in Dataset 1 colored by their correlation with a given cluster medoid (controlling for the other two medoids). Cluster-1- and Cluster-2-like responses are present throughout frontal and temporal areas (with Cluster 1 responses having a slightly higher concentration in the temporal pole and Cluster 2 responses having a slightly higher concentration in the superior temporal gyrus (STG)), whereas Cluster-3-like responses are localized to the posterior STG.

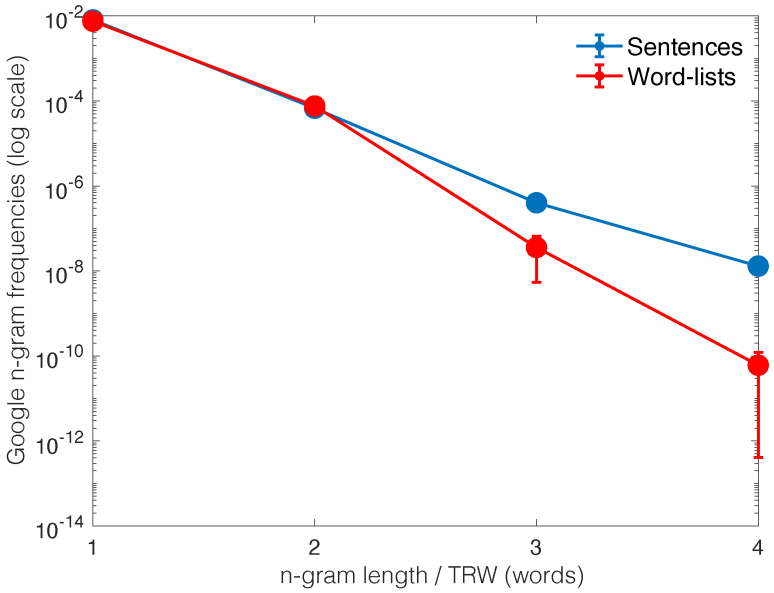

Figure S5 – N-gram frequencies of sentences and word-lists diverge with n-gram length. N-gram frequencies were extracted from the Google n-gram online platform (https://books.google.com/ngrams/), averaging across Google books corpora between the years 2010 and 2020. For each individual word, n-gram frequency for n=1 is the frequency of that individual word in the corpus, for n=2 is the frequency of the bigram (sequence of 2 words) ending in, and including, that word, for n=3 is the frequency of the trigram (sequence of 3 words) ending in, and including, that word, etc. Sequences that were not found in the corpus were assigned a value of 0. Results are only presented until n=4 because for n>4 most of the word sequences, both from the Sentence and Word-list conditions were not found in the corpora. The plot shows that the difference between the log n-gram values for the sentences and wordlists grows as a function of N.

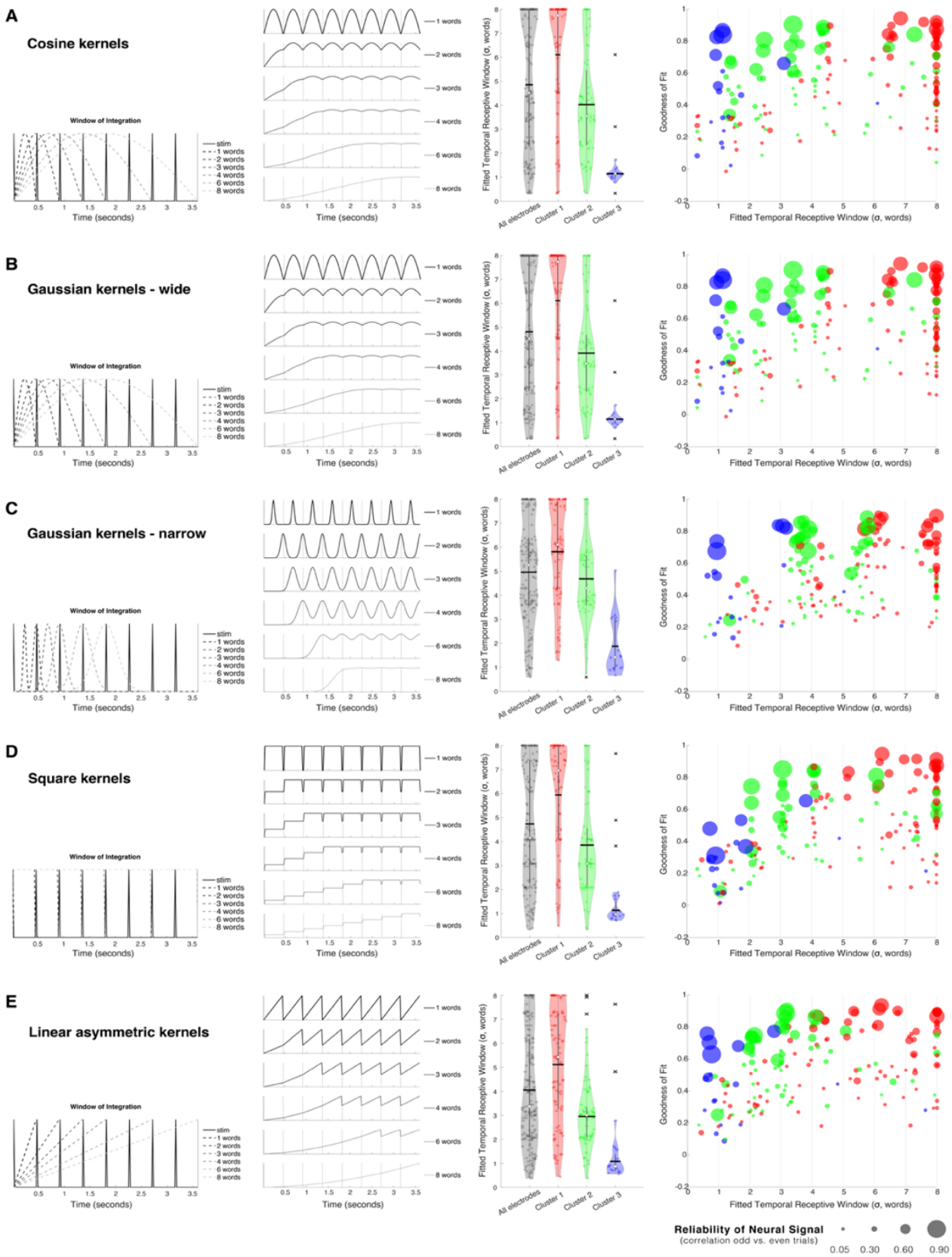
A
Cosine kernels
B
Gaussian kernels - wide
C
Gaussian kernels - narrow
D
Square kernels
E
Linear asymmetric kernels
Window of Integration
stim
1 words
2 words
3 words
4 words
6 words
8 words
Time (seconds)
Fitted Temporal Receptive Window (σ, words)
All electrodes
Cluster 1
Cluster 2
Cluster 3
Goodness of Fit
Fitted Temporal Receptive Window (σ, words)
Reliability of Neural Signal
(correlation odd vs. even trials)
0.05
0.30
0.60
0.90

Figure S6 – Temporal receptive window (TRW) estimates with kernels of different shapes. Modulation of TRW by cluster does not depend on the choice of kernel. TRW model was fitted using five different kernel shapes: cosine (**A**), "wide" Gaussian (Gaussian curves with a standard deviation of $\sigma/2$ that were truncated at +/- 1 standard deviation, as used in **Figure 4**; **B**), "narrow" Gaussian (Gaussian curves with a standard deviation of $\sigma/16$ that were truncated at +/- 8 standard deviations; **C**), a square (i.e., boxcar) function (1 for the entire window; **D**) and a linear asymmetric function (linear function with a value of 0 initially and a value of 1 at the end of the window; **E**). For each kernel (**A-E**), the plots represent (left to right, all details are identical to **Figure 4** in the manuscript): 1) The kernel shapes for TRW = 1, 2, 3, 4, 6 and 8 words, superimposed on the simplified stimulus train; 2) The simulated neural signals for each of those TRWs; 3) violin plots of best fitted TRW values across electrodes (each dot represents and electrode) for all electrodes (black), or electrodes from only Clusters 1 (red) 2 (green) or 3 (blue); and 4) Estimated TRW as a function of goodness of fit. Each dot is an electrode, its size represents the reliability of its neural response, computed via correlation between the mean signals when using only odd vs. only even trials, x-axis is the electrode's best fitted TRW, y-axis is the goodness of fit, computed via correlation between the neural signal and the closest simulated signal. For all kernels the TRWs show a decreasing trend from Cluster 1 to 3.

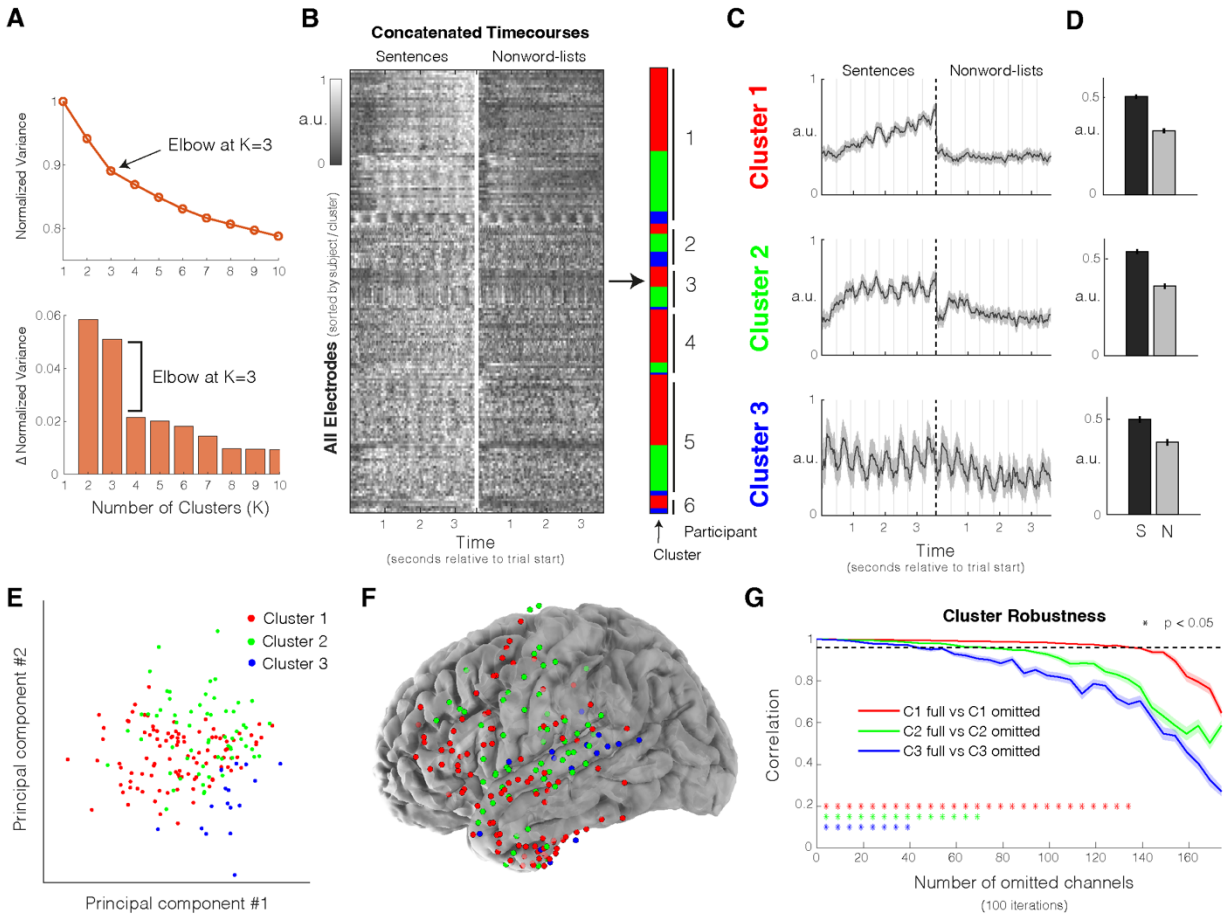

Figure S7 – Dataset 1 k-medoids clustering results with only S-N conditions. A) Search for optimal k using the "elbow method". Top: variance (sum of the distances of all electrodes to their assigned cluster center) normalized by the variance when k=1 as a function of k (normalized variance (NV)). Bottom: change in NV as a function of k (NV(k+1) – NV(k)). After k=3 the change in variance becomes more moderate, suggesting that 3 clusters appropriately describe Dataset 1 when using only the responses to sentences and nonwords (as was the case when all four conditions were used). **B)** Clustering mean electrode responses (only S+N, importantly) using k-medoids (k=3) with a correlation-based distance. Shading of the data matrix reflects normalized high-gamma power (70-150Hz). **C)** Average timecourse by cluster. Shaded areas around the signal reflect a 99% confidence interval over electrodes. Clusters 1-3 show strong similarity to the clusters reported in **Figure 2**. **D)** Mean condition responses by cluster. Error bars reflect standard error of the mean over electrodes. **E)** Electrode responses visualized on their first two principal components, colored by cluster. **F)** Anatomical distribution of clusters across all participants (n=6). **G)** Robustness of clusters electrode omission (random subsets of electrodes were removed in increments of 5). Stars reflect significant similarity with the full dataset ($p<0.05$; evaluated with a permutation test; Methods). Shaded regions reflect standard error of the mean over randomly sampled subsets of electrodes. Relative to when all conditions were used, Cluster 2 is less robust to electrode omission (although still more robust than Cluster 3), suggesting that responses to word-lists and Jabberwocky sentences (both not present here) are particularly important for distinguishing Cluster 2 electrodes from Cluster 1 and 3 electrodes.

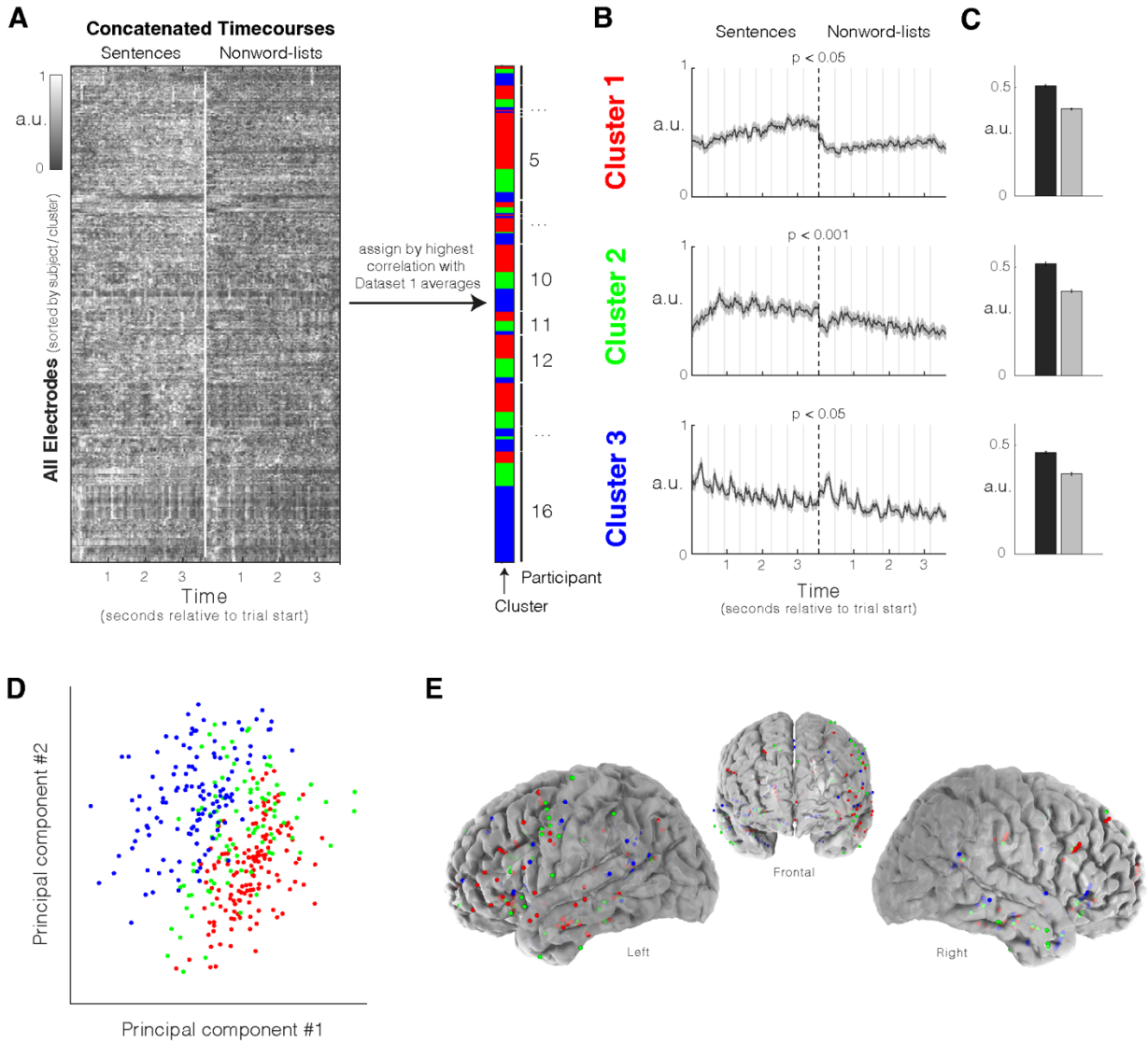

Figure S8 – Dataset 2 electrode assignment to most correlated Dataset 1 cluster. A) Assigning electrodes from Dataset 2 to the most correlated cluster from Dataset 1. Assignment is performed using the correlation with the Dataset 1 cluster average, not the cluster medoid. Shading of the data matrix reflects normalized high-gamma power (70-150Hz). **B)** Average timecourse by cluster. Shaded areas around the signal reflect a 99% confidence interval over electrodes. Under this procedure, all clusters – including Cluster 2 – are more similar to the clusters in Dataset 1 than would be expected by chance (C1: p=0.025, C2: p=0.001, C3: p=0.029; evaluated with a permutation test, Methods). **C)** Mean condition responses by cluster. Error bars reflect standard error of the mean over electrodes. **E)** Electrode responses visualized on their first two principal components, colored by cluster. **F)** Anatomical distribution of clusters across all participants (n=16).

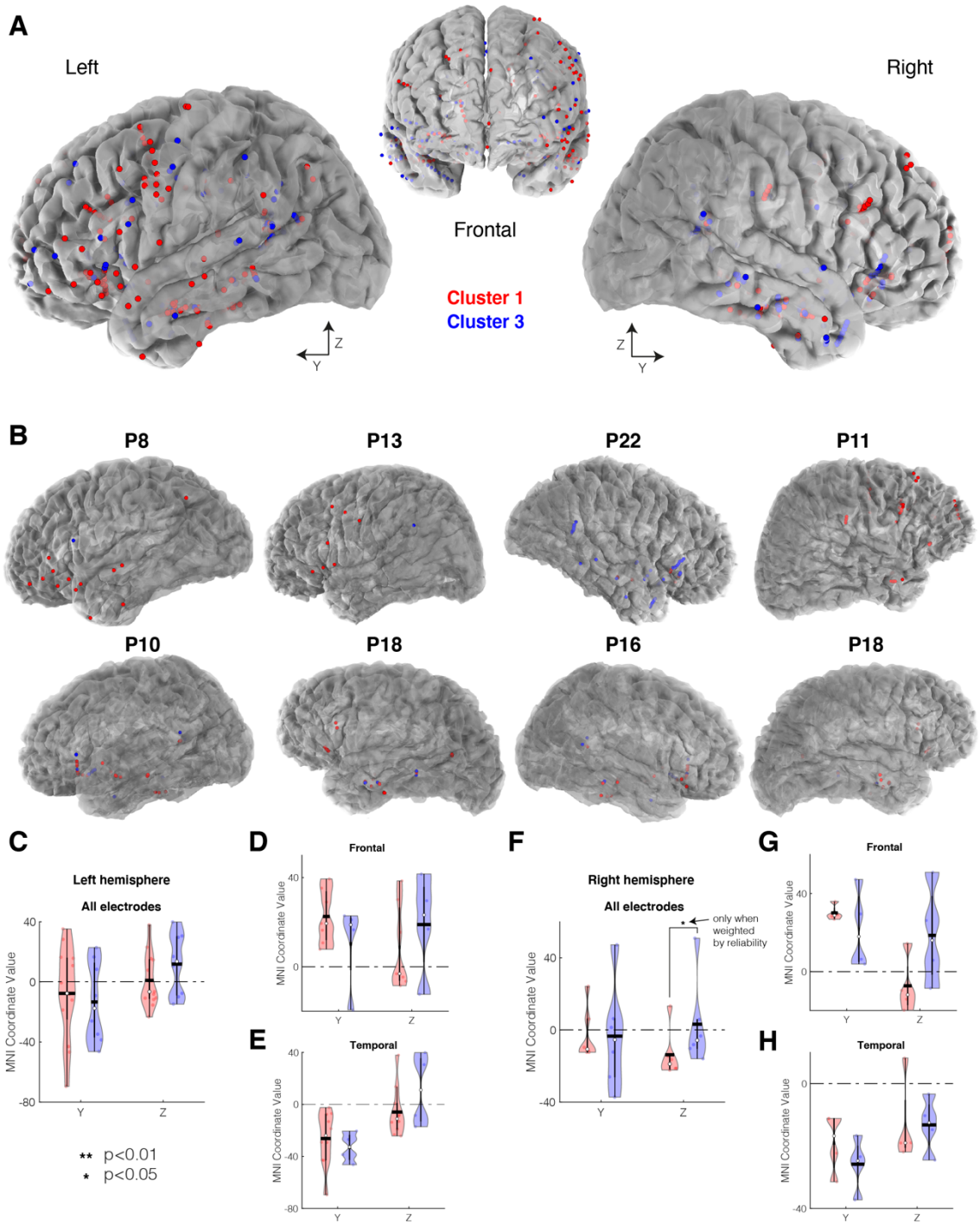

Figure S9 – Anatomical distribution of the clusters in Dataset 2. Anatomical distribution of language-responsive electrodes in Dataset 2 across all subjects in MNI space, colored by cluster. Only Clusters 1 and 3 (those from Dataset 1 that replicate to Dataset 2) are shown. **B)** Anatomical distribution of language-responsive electrodes in subject-specific space for eight sample participants. **C-H)** Violin plots of MNI coordinate values for Clusters 1 and 3 in the left and right hemisphere (**C-E** and **F-H**, respectively), where plotted points represent the mean of all coordinate values for a given participant and cluster. The mean is plotted with a black horizontal line, and the median is shown with a white circle. Significance is evaluated with a LME model (Methods, **Tables S3** and **S4**). The Cluster 3 posterior bias from Dataset 1 is weakly present but not statistically reliable.

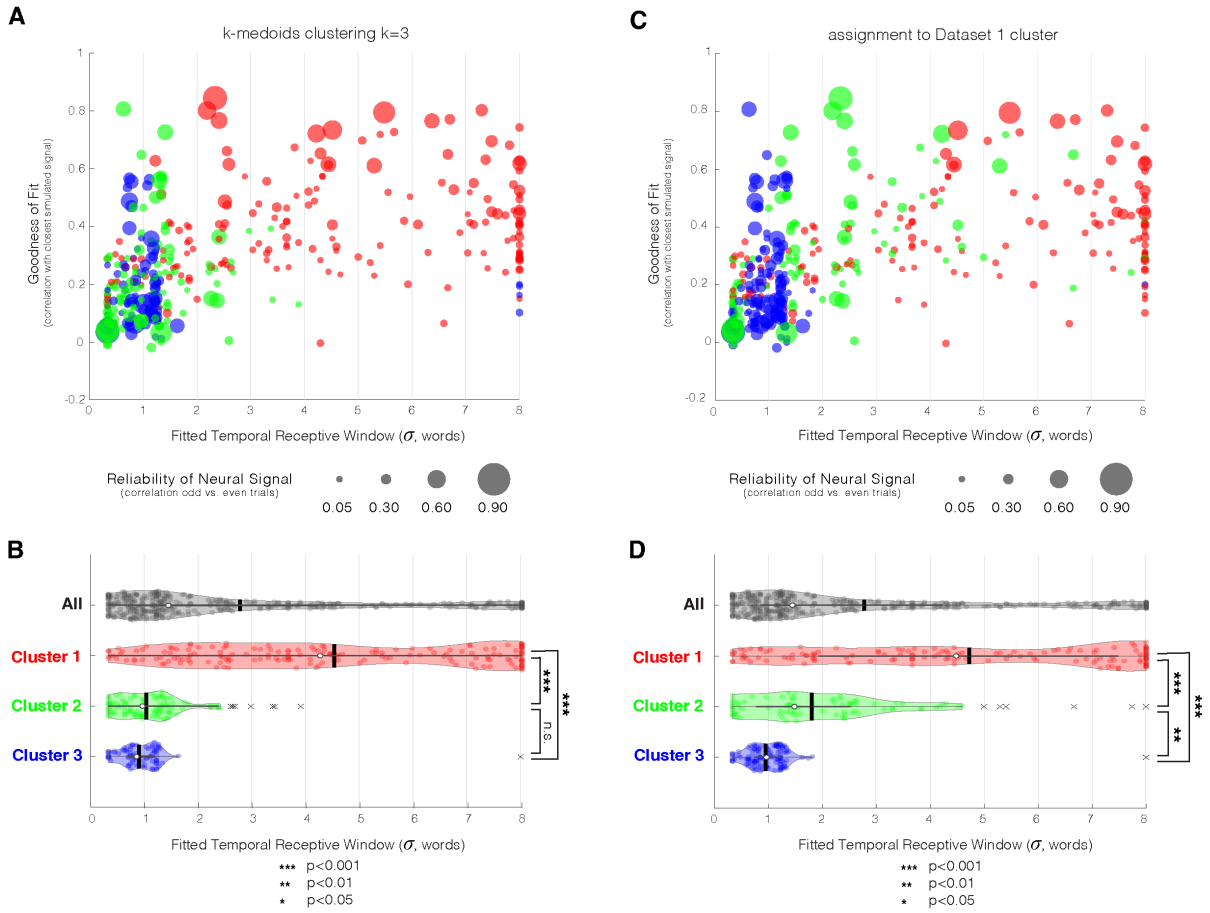

Figure S10 – Estimation of temporal receptive window (TRW) sizes for electrodes in Dataset 2. As in **Figure 4** but for electrodes in Dataset 2. **A)** Best TRW fit (using the toy model from **Figure 4**) for all electrodes colored by cluster (when k-medoids clustering with k=3 is applied, **Figure 6**) and sized by the reliability of the neural signal as estimated by correlating responses to odd and even trials (**Figure 6C**). The 'goodness of fit', or correlation between the simulated and observed neural signal (sentence condition only), is shown on the y-axis. **B)** Estimated TRW sizes across all electrodes (grey) and per cluster (red, green, and blue). Black vertical lines correspond to the mean window size and the white dots correspond to the median. "x" marks indicate outliers (more than 1.5 interquartile ranges above the upper quartile or less than 1.5 interquartile ranges below the lower quartile). Significance values are calculated using a linear mixed-effects model (Methods, **Table S8**). **C-D)** Same as **A** and **B**, respectively, except clusters are assigned by highest correlation with Dataset 1 clusters (**Figure S8**). Under this procedure, Cluster 2 reliably separates from Cluster 3 in terms of its TRW (all ps<0.001, evaluated with a LME model, Methods, **Table S9**).

Name	Estimate	SE	tStat	DF	pValue
C1, Condition S – reference	**0.103**	**0.023**	**4.503**	**10.332**	**0.001**
C2 – relative to C1	0.074	0.038	1.974	11.573	0.073
C3 – relative to C1	**0.239**	**0.080**	**2.971**	**7.464**	**0.019**
Condition W – relative to S	-0.023	0.026	-0.880	681.988	0.38
Condition J – relative to S	-0.036	0.027	-1.338	27.077	0.19
Condition N – relative to S	**-0.060**	**0.027**	**-2.270**	**46.806**	**0.028**
Condition W: C2 relative to C1	-0.026	0.040	-0.657	682.349	0.51
Condition W: C3 relative to C1	0.022	0.063	0.348	682.352	0.73
Condition J: C2 relative to C1	-0.041	0.040	-1.046	677.506	0.30
Condition J: C3 relative to C1	0.007	0.064	0.111	644.768	0.91
Condition N: C2 relative to C1	-0.063	0.040	-1.588	680.554	0.11
Condition N: C3 relative to C1	-0.046	0.063	-0.718	665.329	0.47
C2, Condition S – reference	**0.178**	**0.029**	**6.053**	**11.092**	**0.00008**
C3 – relative to C2	0.164	0.082	2.001	7.518	0.083
C1 – relative to C2	-0.074	0.038	-1.974	11.573	0.073
Condition W – relative to S	-0.049	0.030	-1.614	682.210	0.11
Condition J – relative to S	**-0.078**	**0.031**	**-2.485**	**52.580**	**0.016**
Condition N – relative to S	**-0.123**	**0.031**	**-4.000**	**90.665**	**0.00013**
Condition W: C3 relative to C2	0.048	0.065	0.735	682.350	0.46
Condition W: C1 relative to C2	0.026	0.040	0.657	682.349	0.51
Condition J: C3 relative to C2	0.048	0.065	0.741	669.544	0.46
Condition J: C1 relative to C2	0.041	0.040	1.046	677.506	0.30
Condition N: C3 relative to C2	0.017	0.065	0.262	677.099	0.79
Condition N: C1 relative to C2	0.063	0.040	1.588	680.554	0.11

Table S1A LME results quantifying degree of stimulus locking by cluster. All estimates from the linear mixed-effects model (LME) regressing the locking value (Methods) on the categorical variables of cluster (3 levels) and condition (4 levels for sentences (S), word-lists (W), jabberwocky (J), nonword-lists (N), Methods), including their interaction, all grouped by the random variable of participant. Model formula: *Locking ~ cluster*condition + (cluster|participant) + (condition|participant)*). The Satterthwaite Method was used to estimate the degrees of freedom (DF) due to our small sample size. Implemented with Matlab *fitlme* routine. Semicolon represents interactions. The intercept represents one level of each of the categorical variables and is denoted by "reference". The models are reference-coded such that all estimate values are evaluated and compared statistically to the intercept/reference. Two models are presented, separated by a horizontal line. The only difference between the models regards the level of the categorical variable 'Cluster' that is assigned to the reference. In the first model the intercept/reference is for Cluster 1 (C1), and in the second model it is Cluster 2 (C2). We used the second model in order to obtain the statistical comparisons between clusters 2 and 3. The estimate magnitudes show a trend for stimulus locking by cluster: C1<C2<C3, but the only pairwise comparison that reached significance was of Cluster 3 to 1 ($p<0.05$) and the other comparisons were marginally significant ($p<0.1$). Estimate magnitudes further show a trend for stimulus locking by Condition: S>W>J>N, but the only pairwise comparison that reached significance was S vs. N ($p<0.05$) in the first model, and J vs. S in the second model ($p<0.001$). No interaction terms were significant. An additional ANOVA test for LME revealed a significant main effect for cluster ($F(2,9.13)=5.4$, $p<0.05$) and the main effect for condition as well as the interaction term did not reach significance . See **Figure 5**.

Name	FStat	DF1	DF2	pValue
(Intercept)	**20.3**	**1**	**10.33**	**0.0010**
Cluster	**5.4**	**2**	**9.13**	**0.028**
Condition	1.9	3	41.84	0.15
Cluster : Condition	0.6	6	670.00	0.73

Table S1B ANOVA for the LME results presented in Table S1A. ANOVA for LME was run on the first model presented in Table S1A. These results reveal that the main effect of Cluster was overall significant ($p<0.05$), but the main effect of Condition as well as the interaction between cluster and condition did not reach significance.

Dataset	Coordinate	Name	Estimate	SE	tStat	DF	pValue
Dataset 1	y	C1 - reference	1.36	4.09	0.33	5.16	0.75
Dataset 1	y	C2 - relative to C1	-2.93	3.62	-0.81	26.14	0.42
Dataset 1	**y**	**C3 - relative to C1**	**-20.91**	**5.93**	**-3.53**	**63.46**	**0**
Dataset 1	y	C2 - reference	-1.57	3.65	-0.43	5.34	0.68
Dataset 1	**y**	**C3 - relative to C2**	**-17.98**	**5.9**	**-3.05**	**159.46**	**0**
Dataset 1	y	C1 - relative to C2	2.93	3.62	0.81	26.14	0.42
Dataset 1	z	C1 - reference	-4.4	4.84	-0.91	4.43	0.41
Dataset 1	z	C2 - relative to C1	16.87	7.69	2.19	4.54	0.09
Dataset 1	z	C3 - relative to C1	10.64	8.57	1.24	7.87	0.25
Dataset 1	**z**	**C2 - reference**	**12.47**	**4.18**	**2.98**	**6.04**	**0.02**
Dataset 1	z	C3 - relative to C2	-6.22	7.78	-0.8	29.47	0.43
Dataset 1	z	C1 - relative to C2	-16.87	7.69	-2.19	4.54	0.09

Table S2A – LME results comparing MNI coordinates of the 3 clusters, Dataset 1, Left hemisphere. All estimates from the linear mixed-effects model (LME) regressing the y (posterior-anterior) and z (inferior-superior) MNI coordinates (Methods) on the categorical variable of cluster (3 levels) grouped by the random variable of participant. Model formula: *MNI coordinate ~ cluster + (cluster|participant).* Details are similar to Table S1A. The y-coordinate of Cluster 3 was significantly different from Clusters 1 and 2 (ps<0.01). All the other comparisons did not reach significance. See **Figure 6**.

Dataset	Coordinate	Name	Estimate	SE	tStat	DF	pValue
Dataset 1	y	C1 - reference	4.9	5.6	0.9	5.2	0.413759
Dataset 1	**y**	**C2 - relative to C1**	**-8.3**	**3.7**	**-2.2**	**38.1**	**0.031376**
Dataset 1	**y**	**C3 - relative to C1**	**-27.9**	**5.4**	**-5.1**	**166.1**	**8.00E-07**
Dataset 1	y	C2 - reference	-3.4	4.9	-0.7	4.9	0.52027
Dataset 1	**y**	**C3 - relative to C2**	**-19.5**	**5.5**	**-3.6**	**64.7**	**0.000706**
Dataset 1	**y**	**C1 - relative to C2**	**8.3**	**3.7**	**2.2**	**38.1**	**0.031376**
Dataset 1	z	C1 - reference	-1.3	3.4	-0.4	3	0.732998
Dataset 1	**z**	**C2 - relative to C1**	**19.2**	**5.1**	**3.8**	**2.5**	**0.045907**
Dataset 1	z	C3 - relative to C1	14.8	7.5	2	2.5	0.162557
Dataset 1	**z**	**C2 - reference**	**17.9**	**3.9**	**4.6**	**1.7**	**0.059805**
Dataset 1	z	C3 - relative to C2	-4.4	8.7	-0.5	1.7	0.672232
Dataset 1	**z**	**C1 - relative to C2**	**-19.2**	**5.1**	**-3.8**	**2.5**	**0.045907**

Table S2B – Same as Table S2A but electrodes were weighted by reliability.

Dataset	Coordinate	Name	Estimate	SE	tStat	DF	pValue
Dataset 1	y	C1 - reference	9.6	7.6	1.3	5.3	0.26
Dataset 1	y	C2 - relative to C1	-5.6	6.0	-0.9	5.0	0.40
Dataset 1	y	C3 - relative to C1	-10.9	11.0	-1.0	2.4	0.41
Dataset 1	y	C2 - reference	4.0	5.0	0.8	4.7	0.46
Dataset 1	y	C3 - relative to C2	-5.3	11.0	-0.5	4.5	0.65
Dataset 1	y	C1 - relative to C2	5.6	6.0	0.9	5.0	0.40
Dataset 1	**z**	**C1 - reference**	**13.3**	**4.7**	**2.8**	**6.7**	**0.03**
Dataset 1	z	C2 - relative to C1	6.2	7.7	0.8	4.7	0.46
Dataset 1	z	C3 - relative to C1	8.5	11.5	0.7	10.1	0.48
Dataset 1	z	C2 - reference	19.5	9.0	2.2	4.0	0.10
Dataset 1	z	C3 - relative to C2	2.3	14.5	0.2	4.5	0.88
Dataset 1	z	C1 - relative to C2	-6.2	7.7	-0.8	4.7	0.46

Table S2C – Same as Table S2A but only frontal electrodes.

Dataset	Coordinate	Name	Estimate	SE	tStat	DF	pValue
Dataset 1	y	C1 - reference	-3.8	4.5	-0.8	3.7	0.45
Dataset 1	y	C2 - relative to C1	0.4	4.4	0.1	42.8	0.93
Dataset 1	**y**	**C3 - relative to C1**	**-22.3**	**6.9**	**-3.2**	**26.6**	**0.003**
Dataset 1	y	C2 - reference	-3.4	5.6	-0.6	3.8	0.58
Dataset 1	**y**	**C3 - relative to C2**	**-22.7**	**7.5**	**-3.0**	**17.6**	**0.008**
Dataset 1	y	C1 - relative to C2	-0.4	4.4	-0.1	42.8	0.93
Dataset 1	z	C1 - reference	-6.4	13.8	-0.5	3.6	0.67
Dataset 1	z	C2 - relative to C1	18.2	7.5	2.4	1.7	0.16
Dataset 1	z	C3 - relative to C1	10.4	15.9	0.7	1.7	0.59
Dataset 1	z	C2 - reference	11.8	9.5	1.2	3.1	0.30
Dataset 1	z	C3 - relative to C2	-7.8	11.6	-0.7	1.7	0.58
Dataset 1	z	C1 - relative to C2	-18.2	7.5	-2.4	1.7	0.16

Table S2D – Same as Table S2A but only temporal electrodes.

Dataset	Coordinate	Name	Estimate	SE	tStat	DF	pValue
Dataset 2	y	C1 - reference	-5.3	7.5	-0.7	8.9	0.5
Dataset 2	y	C2 - relative to C1	-7.2	10.4	-0.7	7.2	0.5
Dataset 2	y	C3 - relative to C1	-1.5	11.0	-0.1	7.8	0.9
Dataset 2	y	C2 - reference	-12.6	7.8	-1.6	10.4	0.1
Dataset 2	y	C3 - relative to C2	5.7	8.3	0.7	9.4	0.5
Dataset 2	y	C1 - relative to C2	7.2	10.4	0.7	7.2	0.5
Dataset 2	z	C1 - reference	3.1	4.2	0.7	12.6	0.5
Dataset 2	**z**	**C2 - relative to C1**	**12.8**	**3.9**	**3.3**	**183.7**	**0.001**
Dataset 2	z	C3 - relative to C1	7.3	5.9	1.2	30.1	0.2
Dataset 2	**z**	**C2 - reference**	**15.8**	**4.6**	**3.4**	**12.0**	**0.005**
Dataset 2	z	C3 - relative to C2	-5.4	5.9	-0.9	38.8	0.4
Dataset 2	**z**	**C1 - relative to C2**	**-12.8**	**3.9**	**-3.3**	**183.7**	**0.001**

Table S3A – LME results comparing coordinates of the 3 clusters, Dataset 2, Left hemisphere.
Similar to Table S2A but for Dataset 2, left hemisphere electrodes. The only significant comparison was the z-coordinate of Cluster 2 relative to Clusters 1 ($p<0.01$). See **Figure S5**.

Dataset	Coordinate	Name	Estimate	SE	tStat	DF	pValue
Dataset 2	y	C1 - reference	-0.1	6.3	0.0	7.2	0.98
Dataset 2	y	C2 - relative to C1	-16.2	11.6	-1.4	6.7	0.21
Dataset 2	y	C3 - relative to C1	-4.6	10.4	-0.4	5.1	0.68
Dataset 2	y	C2 - reference	-16.3	8.5	-1.9	8.4	0.09
Dataset 2	y	C3 - relative to C2	11.6	8.9	1.3	9.5	0.23
Dataset 2	y	C1 - relative to C2	16.2	11.6	1.4	6.7	0.21
Dataset 2	z	C1 - reference	4.2	5.0	0.8	11.7	0.42
Dataset 2	**z**	**C2 - relative to C1**	**15.4**	**5.8**	**2.6**	**11.0**	**0.02**
Dataset 2	z	C3 - relative to C1	14.0	7.2	1.9	8.2	0.09
Dataset 2	**z**	**C2 - reference**	**19.5**	**4.7**	**4.2**	**9.3**	**0.002**
Dataset 2	z	C3 - relative to C2	-1.4	5.9	-0.2	11.4	0.82
Dataset 2	**z**	**C1 - relative to C2**	**-15.4**	**5.8**	**-2.6**	**11.0**	**0.02**

Table S3B – Same as Table S3A but electrodes are weighted by reliability.

Dataset	Coordinate	Name	Estimate	SE	tStat	DF	pValue
Dataset 2	**y**	**C1 - reference**	**21.1**	**4.3**	**4.9**	**5.0**	**0.0045**
Dataset 2	y	C2 - relative to C1	-1.0	7.4	-0.1	8.8	0.9
Dataset 2	y	C3 - relative to C1	-10.5	10.4	-1.0	5.1	0.4
Dataset 2	**y**	**C2 - reference**	**20.1**	**5.8**	**3.4**	**7.1**	**0.011**
Dataset 2	y	C3 - relative to C2	-9.4	8.9	-1.1	18.5	0.3
Dataset 2	y	C1 - relative to C2	1.0	7.4	0.1	8.8	0.9
Dataset 2	z	C1 - reference	11.7	6.6	1.8	7.5	0.11
Dataset 2	z	C2 - relative to C1	6.2	6.2	1.0	6.5	0.4
Dataset 2	z	C3 - relative to C1	6.1	9.4	0.6	5.2	0.5
Dataset 2	**z**	**C2 - reference**	**18.0**	**5.5**	**3.3**	**6.7**	**0.015**
Dataset 2	z	C3 - relative to C2	-0.2	8.2	0.0	7.8	1.0
Dataset 2	z	C1 - relative to C2	-6.2	6.2	-1.0	6.5	0.4

Table S3C – Same as Table S3A but only frontal electrodes.

Dataset	Coordinate	Name	Estimate	SE	tStat	DF	pValue
Dataset 2	**y**	**C1 - reference**	**-24.1**	**5.4**	**-4.4**	**6.2**	**0.0040**
Dataset 2	y	C2 - relative to C1	-12.8	7.0	-1.8	8.1	0.10
Dataset 2	y	C3 - relative to C1	-4.5	9.8	-0.5	7.6	0.66
Dataset 2	**y**	**C2 - reference**	**-36.9**	**4.0**	**-9.3**	**39.1**	**2E-11**
Dataset 2	y	C3 - relative to C2	8.3	8.6	1.0	52.8	0.34
Dataset 2	y	C1 - relative to C2	12.8	7.0	1.8	8.1	0.10
Dataset 2	z	C1 - reference	-4.0	4.9	-0.8	5.5	0.45
Dataset 2	z	C2 - relative to C1	8.6	5.4	1.6	46.8	0.11
Dataset 2	z	C3 - relative to C1	12.5	10.2	1.2	6.0	0.27
Dataset 2	z	C2 - reference	4.6	4.7	1.0	7.4	0.36
Dataset 2	z	C3 - relative to C2	3.9	10.6	0.4	5.6	0.72
Dataset 2	z	C1 - relative to C2	-8.6	5.4	-1.6	46.8	0.11

Table S3D – Same as Table S3A but only temporal electrodes.

Dataset	Coordinate	Name	Estimate	SE	tStat	DF	pValue
Dataset 2	y	C1 - reference	2.49	7.18	0.35	7.70	0.74
Dataset 2	**y**	**C2 - relative to C1**	**-17.17**	**7.02**	**-2.45**	**11.13**	**0.03**
Dataset 2	y	C3 - relative to C1	-7.00	7.52	-0.93	8.64	0.38
Dataset 2	**y**	**C2 - reference**	**-14.68**	**4.39**	**-3.35**	**3.20**	**0.04**
Dataset 2	y	C3 - relative to C2	10.18	7.84	1.30	2.29	0.31
Dataset 2	**y**	**C1 - relative to C2**	**17.17**	**7.02**	**2.45**	**11.13**	**0.03**
Dataset 2	z	C1 - reference	-8.56	5.94	-1.44	6.44	0.20
Dataset 2	z	C2 - relative to C1	5.57	4.97	1.12	2.68	0.35
Dataset 2	z	C3 - relative to C1	14.76	5.99	2.46	4.09	0.07
Dataset 2	z	C2 - reference	-2.98	6.38	-0.47	2.47	0.68
Dataset 2	z	C3 - relative to C2	9.18	4.69	1.96	0.74	0.36
Dataset 2	z	C1 - relative to C2	-5.57	4.97	-1.12	2.68	0.35

Table S4A – LME results comparing coordinates of the 3 clusters, Dataset 2, Right hemisphere. Similar to Table S3A but for right-hemisphere electrodes. The significant comparisons were of the y-coordinates of Cluster 2 vs. 1 ($p<0.05$). See **Figure S5**.

Dataset	Coordinate	Name	Estimate	SE	tStat	DF	pValue
Dataset 2	y	C1 - reference	3.7	9.3	0.4	8.1	0.70
Dataset 2	**y**	**C2 - relative to C1**	**-17.2**	**8.5**	**-2.0**	**72.4**	**0.047**
Dataset 2	y	C3 - relative to C1	-4.5	9.3	-0.5	10.9	0.64
Dataset 2	y	C2 - reference	-13.4	7.4	-1.8	1.6	0.24
Dataset 2	y	C3 - relative to C2	12.7	6.3	2.0	1.3	0.25
Dataset 2	**y**	**C1 - relative to C2**	**17.2**	**8.5**	**2.0**	**72.4**	**0.047**
Dataset 2	z	C1 - reference	-8.0	6.9	-1.2	6.5	0.29
Dataset 2	z	C2 - relative to C1	6.9	7.5	0.9	2.1	0.45
Dataset 2	**z**	**C3 - relative to C1**	**16.4**	**6.0**	**2.8**	**7.2**	**0.027**
Dataset 2	z	C2 - reference	-1.1	8.1	-0.1	2.6	0.90
Dataset 2	z	C3 - relative to C2	9.5	5.2	1.8	0.4	0.54
Dataset 2	z	C1 - relative to C2	-6.9	7.5	-0.9	2.1	0.45

Table S4B – Same as Table S4A but electrodes are weighted by reliability. The significant comparisons were of the y-coordinates of Cluster 2 vs. 1, and the z-coordinate of Cluster 3 relative to 1 ($ps<0.05$).

Dataset	Coordinate	Name	Estimate	SE	tStat	DF	pValue
Dataset 2	**y**	**C1 - reference**	**33.9**	**3.4**	**9.9**	**40.9**	**2E-12**
Dataset 2	y	C2 - relative to C1	-22.2	13.9	-1.6	1.7	0.27
Dataset 2	y	C3 - relative to C1	-13.2	9.6	-1.4	3.2	0.26
Dataset 2	y	C2 - reference	11.7	13.5	0.9	1.6	0.50
Dataset 2	y	C3 - relative to C2	9.1	15.2	0.6	4.0	0.58
Dataset 2	y	C1 - relative to C2	22.2	13.9	1.6	1.7	0.27
Dataset 2	z	C1 - reference	-3.3	8.0	-0.4	2.8	0.71
Dataset 2	z	C2 - relative to C1	-4.2	10.9	-0.4	2.9	0.73
Dataset 2	z	C3 - relative to C1	23.4	14.7	1.6	2.3	0.23
Dataset 2	z	C2 - reference	-7.5	6.9	-1.1	6.4	0.31
Dataset 2	z	C3 - relative to C2	27.6	15.4	1.8	4.4	0.14
Dataset 2	z	C1 - relative to C2	4.2	10.9	0.4	2.9	0.73

Table S4C – Same as Table S4A but only frontal electrodes. No significant comparisons.

Dataset	Coordinate	Name	Estimate	SE	tStat	DF	pValue
Dataset 2	**y**	**C1 - reference**	**-17.5**	**5.6**	**-3.1**	**5.8**	**0.021**
Dataset 2	y	C2 - relative to C1	-3.7	7.5	-0.5	13.4	0.63
Dataset 2	y	C3 - relative to C1	-6.4	6.7	-1.0	28.7	0.35
Dataset 2	**y**	**C2 - reference**	**-21.2**	**6.4**	**-3.3**	**2.9**	**0.048**
Dataset 2	y	C3 - relative to C2	-2.7	6.1	-0.4	6.6	0.68
Dataset 2	y	C1 - relative to C2	3.7	7.5	0.5	13.4	0.63
Dataset 2	z	C1 - reference	-10.7	7.7	-1.4	3.3	0.25
Dataset 2	z	C2 - relative to C1	-4.1	9.4	-0.4	3.0	0.69
Dataset 2	z	C3 - relative to C1	-1.6	8.9	-0.2	5.4	0.87
Dataset 2	z	C2 - reference	-14.8	4.9	-3.0	0.6	0.30
Dataset 2	z	C3 - relative to C2	2.5	5.9	0.4	3.1	0.70
Dataset 2	z	C1 - relative to C2	4.1	9.4	0.4	3.0	0.69

Table S4D – Same as Table S4A but only temporal electrodes. No significant comparisons.

Name	Estimate	SE	tStat	DF	pValue
C1 - reference	**6.5**	**0.5**	**12.6**	**5.1**	**5.2E-05**
C2 - relative to C1	**-2.5**	**0.6**	**-4.0**	**3.6**	**0.020**
C3 - relative to C1	**-5.1**	**0.6**	**-8.1**	**8.7**	**2.6E-05**
C2 - reference	**4.0**	**0.5**	**7.9**	**4.3**	**0.0010**
C3 - relative to C2	**-2.5**	**0.6**	**-4.0**	**8.0**	**0.0040**
C1 - relative to C2	**2.5**	**0.6**	**4.0**	**3.6**	**0.020**

Table S5 – LME results comparing temporal receptive windows (TRW) of the 3 clusters, Dataset 1. All estimates from the linear mixed-effects model (LME) regressing the estimated temporal receptive window (TRW) size (Methods) on the categorical variable of cluster (3 levels) grouped by the random variable of participant. Model formula: *trw ~ cluster + (cluster|participant).* The Satterthwaite Method was used to estimate the degrees of freedom (DF) due to our small sample size. Details are similar to Table S1A. All comparisons were statistically significant: Cluster 2 had a smaller TRW compared to Cluster 1, and Cluster 3 had the smallest trw compared to both other clusters (all ps<0.01). See **Figure 4**.

Name	Estimate	SE	tStat	DF	pValue
TRW C1 - reference	**2.6**	**0.3**	**8.6**	**2.2**	**0.010**
TRW C2 - relative to C1	**-1.0**	**0.3**	**-4.0**	**3.2**	**0.025**
TRW C3 - relative to C1	-2.1	0.5	-4.4	1.7	0.066
TRW C2 - reference	**1.6**	**0.2**	**7.8**	**2.9**	**0.005**
TRW C3 - relative to C2	-1.1	0.4	-2.7	3.4	0.066
TRW C1 - relative to C2	**1.0**	**0.3**	**4.0**	**3.2**	**0.025**

Table S6 – LME results comparing temporal receptive windows (TRW) of the 3 clusters, Dataset 1, only participants with the faster presentation rate (450 ms, n=3). Similar to Table S5, but only participants with the faster presentation rate (450 ms, n=3). All comparisons are significant (ps<0.01). Note that this analysis includes only 3 participants and after the Satterthwaite approximation has very low degrees-of-freedom, resulting in a very low statistical power. Furthermore, this low number of degrees-of-freedom does not allow to run the ANOVA for LME, which we would need to run in order to test for the significance of the main effect of cluster, beyond comparisons of pairs of clusters.

Name	Estimate	SE	tStat	DF	pValue
TRW C1 - reference	**5.2**	**0.4**	**13.6**	**2.6**	**0.002**
TRW C2 - relative to C1	-2.3	0.9	-2.4	2.0	0.13
TRW C3 - relative to C1	**-3.7**	**0.8**	**-4.9**	**2.2**	**0.034**
TRW C2 - reference	**2.9**	**0.6**	**4.5**	**2.0**	**0.045**
TRW C3 - relative to C2	-1.4	0.7	-2.1	1.3	0.24
TRW C1 - relative to C2	2.3	0.9	2.4	2.0	0.13

Table S7 – LME results comparing temporal receptive windows (TRW) of the 3 clusters, Dataset 1, only participants with the slower presentation rate (700 ms, n=3). Similar to Table S6, but only

participants with the slower presentation rate (700 ms, n=3). The trw estimates show the same trend as above (trw C1 > C2 > C3) but only C3 relative to C1 reached significance (p<0.05). Note that this analysis includes only 3 participants and after the Satterthwaite approximation has very low degrees-of-freedom, resulting in a very low statistical power. Furthermore, this low number of degrees-of-freedom does not allow to run the ANOVA for LME, which we would need to run in order to test for the significance of the main effect of cluster, beyond comparisons of pairs of clusters.

Name	Estimate	SE	tStat	DF	pValue
TRW C1 - reference	**4.5**	**0.3**	**13.4**	**7.6**	**1E-06**
TRW C2 - relative to C1	**-3.3**	**0.4**	**-8.5**	**10.0**	**7E-06**
TRW C3 - relative to C1	**-3.3**	**0.3**	**-9.6**	**28.7**	**2E-10**
TRW C2 - reference	**1.2**	**0.2**	**6.5**	**217.7**	**6E-10**
TRW C3 - relative to C2	0.0	0.3	0.1	15.3	0.92
TRW C1 - relative to C2	**3.3**	**0.4**	**8.5**	**10.0**	**7E-06**

Table S8 – LME results comparing temporal receptive windows (TRW) of the 3 clusters, Dataset 2. Similar to Table S5, but for Dataset 2 using the first 8 words per each trial. The TRW of C2 is smaller than C1 (p<0.0001) but the same as of C3. See **Figure S10A-B**.

Name	Estimate	SE	tStat	DF	pValue
TRW C1 – reference	**4.50**	**0.29**	**15.5**	**10.2**	**2.0E-08**
TRW C2 – relative to C1	**-2.38**	**0.29**	**-8.2**	**8.1**	**3.3E-05**
TRW C3 – relative to C1	**-3.49**	**0.32**	**-10.8**	**14.1**	**3.4E-08**
TRW C2 – reference	**2.12**	**0.27**	**7.8**	**11.2**	**7.2E-06**
TRW C3 – relative to C2	**-1.11**	**0.31**	**-3.6**	**15.6**	**2.5E-03**
TRW C1 – relative to C2	**2.38**	**0.29**	**8.2**	**8.1**	**3.3E-05**

Table S9 – LME results comparing temporal receptive windows (TRW) of the 3 clusters, Dataset 2, using 8 words, electrodes assigned to clusters by similarity to Dataset 1 cluster centers. Similar to Table S8, but here the grouping of electrodes to the 3 clusters was done by assigning each electrode in Dataset 2 to a cluster by its highest correlation with the average cluster response profiles from Dataset 1. All comparisons were statistically significant: Cluster 2 had a smaller TRW compared to Cluster 1, and Cluster 3 had the smallest TRW compared to both other clusters (all ps<0.001). See **Figure S10C-D**.